INL/MIS-23-74144

Flow friction in a wide rectangular duct with a beveled inlet

April 2024

Informal notes of fundamental fluid physics studies

Konner M. Casanova, Michael A. Echevarria, Glenn E. McCreery,
Steven L. Heath, Brian G. Williams, Richard R. Schultz,
Idaho State University, Pocatello, Idaho

Kevin P. Nolan
University College Dublin, Dublin, Ireland

Christian J. Kähler
Universität der Bundewehr, München, Deutschland,

Masahiro Kawaji and
City College of New York, New York, N. Y.

Donald M. McEligot
Idaho National Laboratory, Idaho Falls, Idaho

INL is a U.S. Department of Energy National Laboratory
operated by Battelle Energy Alliance, LLC

Page intentionally left blank

INL/MIS-23-74144

17 April 2024

Informal notes of fundamental fluid physics studies

Flow friction in a wide rectangular duct with a beveled inlet

Konner M. Casanova[1], Michael A. Echevarria[1], Glenn E. McCreery[1], Steven L. Heath[1], Brian G. Williams[1], Richard R. Schultz[1], Kevin P. Nolan[3], Christian J. Kähler[4], Masahiro Kawaji[5] and Donald M. McEligot[2]

[1] Idaho State Univ., Pocatello, Idaho

[2] Idaho National Laboratory, Idaho Falls, Idaho

[3] University College Dublin, Dublin, Ireland

[4] Uni. der Bundeswehr, München, Deutschland

[5] City College of New York, New York, N. Y.

Abstract

Fundamental streamwise pressure distributions were measured at Idaho State University to address a primary objective of obtaining insight into the apparent evolution of air flow regimes at moderate Reynolds numbers in thin, wide rectangular ducts with converging inlets. Ducts of 3.030 and 4.077 mm spacings s (called three and four mm), having non-dimensional lengths of (L/s) ≈ 500.8 and 372.2 and widths (W/s) ≈ 114.6 and 83.2, respectively, were compared. Flow rates ranged from Reynolds numbers based on hydraulic diameter (Re_{Dh}) of about 980 to 10,000 and corresponding non-dimensional downstream pressure gradient parameters ($-K_{p)}$ covered the range 0.038 to 0.0061, respectively. At low Re_{Dh}, *downstream* results for apparent friction factors f_{ds} from both test sections agreed with the laminar fully-developed predictions and for the high Re_{Dh} they showed approximate agreement with the correlation of Beavers, Sparrow and Lloyd [J.Basic.Eng 1971] for fully-developed turbulent flow

in comparable ducts. For three mm, apparently transition started within the test section length for Re_{Dh} greater than about 2700 and for the four mm test section at $Re_{Dh} \approx 3000$. The downstream pressure gradient parameter data indicated that the flow would remain laminar if ($-K_{p,ds}$) is 0.022 or greater for the three mm test section or 0.021 or greater for the four mm one. The *hydraulic entry behavior* of the local apparent friction factor $f_{app}\{x\}$ of the constant cross-section duct downstream of the end of the inlet bevel *showed apparently laminar flow initially for all experiments*. These entry data followed (above) the numerical predictions of Schade and McEligot [IJHMT 1971] for laminar flow in the entry of an infinitely-wide parallel plate duct with a uniform entry velocity. Examining the data with the streamwise Reynolds number as the ordinate demonstrated that, for $Re_{Dh} \approx 4000$ or greater, transition onset (chosen at the minimum f_{app}) is near constant around $Re_{x,to} \approx 1.7 \times 10^5$. As a consequence, in laminar coordinates the location $x_{to}^*\{Re_{Dh}\} = (x_{to} - x_{bevel}) /(sRe_{Dh})$ systematically decreases as Re_{Dh} increases. A secondary objective --- to assess design-style computational fluid dynamics (CFD) predictions from a popular "standard k-ε two-layer turbulence model" --- was also pursued. The *turbulent* k-ε CFD predictions over-predict the entry $f_{app}\{x\}$, by as much as a factor of two, because it is treated as a turbulent flow rather than the laminar entry flow implied by the experiments. The k-ε calculations predict a turbulent entry length of about forty spacings but the experiments indicated it can be much longer. It appears that --- for $Re_{Dh} > \sim 4000$ --- transition would have occurred in the growing near-wall boundary layer. We can obtain further insight into the developing flow phenomena in the hydraulic entry region at these higher Re_{Dh} by considering the transition as "bypass transition," i.e., transition primarily induced by freestream turbulence, and by employing available direct numerical simulations (DNS) of representative bypass transition boundary layers such as those of Zaki and colleagues [JFM 2013, 2016]. For the most part, the present data for flow in the hydraulic entry of a wide rectangular duct show the same flow friction features as the DNS of bypass transition, possibly indicating the presence of the same phenomena / structures.

Keywords Wide rectangular ducts, converging inlets, apparent friction factor measurements, laminar, transitional and turbulent flow, non-dimensional pressure gradient parameter, direct numerical simulation, bypass transition

Nomenclature

{ }	function of
A	cross sectional flow area
APG	adverse pressure gradient
ASL	above sea level
D	diameter
D_h	hydraulic diameter, $4A/\mathcal{p}$
FPG	favorable pressure gradient
G	cross-sectional average mass flux, m/A
k	turbulence kinetic energy, $(\overline{u^2}+\overline{v^2}+\overline{w^2})/2$
L	length, test section length (between bevels); L_{hy}, hydraulic entry length based on $f_{app}\{x\}$
m	mass flow rate; slope
n	exponent
P	pressure
$\mathcal{p}$, P_W	wetted perimeter
R	gas constant
Re'	unit Reynolds number, V_b/ν with units of 1/meter
S	Sutherland constant [White 2 text, sec. 1-3.7, 1991]
s	gap spacing
T	temperature
U	streamwise mean velocity; U_∞, freestream velocity
V	specific volume
V_b	bulk velocity
u, v, w	velocity fluctuations about means in streamwise, wall-normal and spanwise directions, respectively
u_τ	friction velocity, $(\tau_W/\rho)^{1/2}$
W	duct width
x, y	coordinates in streamwise and wall-normal directions, respectively
ZPG	zero (negligible) pressure gradient

Non-dimensional quantities

C	product of f_{fd} and Re_{Dh} for laminar flow
C_f	skin friction coefficient, $2\,\tau_W/(\rho U_\infty{}^2)$
f	duct friction factor; f_{app}, local or pointwise apparent friction factor, $(-2\rho/G^2)$ $(D_h/4)\,d(P + (G^2/\rho))/dx$; f_s, based on wall shear stress, $2\,\tau_W/(\rho V_b{}^2)$; f_{fd}, friction factor in fully-developed flow; f_{ds}, downstream friction factor
K_p	streamwise pressure gradient parameter, $(\nu/(\rho u_\tau{}^3))dp/dx$
K_v	acceleration parameter, $(\nu/V_b{}^2)(dV_b/dx)$
L^*	length, $(x_L - x_{bevel})/(s\,Re_{Dh})$
Re	Reynolds number; Re_{Dh}, based on hydraulic diameter, $V_b D_h/\nu$; Re_x, based on streamwise distance, $U_\infty x/\nu$ or $V_b(x - x_{bevel})/\nu$; Re_θ, based on momentum thickness, $U_\infty\theta/\nu$
$u_{rms}{}^+$	root-mean-squared value of streamwise velocity fluctuations in wall coordinates
x^*	streamwise distance from origin, $(x - x_{bevel})/(s\,Re_{Dh})$
y^+	wall-normal coordinate, yu_τ/ν
Z	compressibility factor, $PV/(RT)$
λ_θ	streamwise acceleration parameter, $(\theta^2/\nu)\,dU_\infty\{x\}/dx$

Greek symbols

γ	intermittency
δ	boundary layer thickness
ε	"homogeneous" dissipation of turbulence kinetic energy used in turbulence models
θ	momentum thickness
μ	absolute viscosity
ν	kinematic viscosity, μ / ρ
ρ	density
τ	shear stress; τ_W, wall shear stress; $\tau_{W,app}$, local apparent wall shear stress, $(-D_h/4)\,d(P + (G^2/\rho))/dx$

Subscripts

0	origin at start of parallel-plate gap; inlet condition

app	apparent
bevel	at end of inlet bevel
BL	boundary layer
BSL	Beavers, Sparrow and Lloyd [J.BasicEng. 1971]
cl	centerplane
D	based on tube diameter; Dh, based on hydraulic diameter
do	developed onset
ds	downstream
duct	duct
fd	fully-developed
in, inlet	inlet condition
L	at end of parallel-plate gap, beginning of exit bevel
lam	laminar
max	maximum
min	minimum
pipe	circular pipe
TL	transverse leg
TS	test section
to	transition onset
tr	transition
w	wall
∞	freestream

1. Introduction

Two classical geometric idealizations for internal duct flow are the circular tube and parallel flat plates, infinitely wide [Schlichting 6 text, 1968; White 2 text, 1991]. The tubular geometry can be approximated closely in practice. On the other hand, infinitely-wide parallel flat plates do not exist; for experiments, wide rectangular ducts are used as approximations. In both cases wide variations of entry geometries are used [Beavers, Sparrow and Magnusson, IJHMT 1970b; Kakac, Shah and Aung handbook 1987; Idelchik handbook 1994]. As seen from the measurements of Beavers, Sparrow and Magnuson [IJHMT 1970b] transitional Reynolds numbers and turbulence development for parallel-plate channels are sensitive to entry

configurations. For the present study. fundamental pressure distribution measurements were obtained for wide rectangular ducts with beveled inlets, simulating the flow channel found between adjacent fuel element blocks in some prismatic gas-cooled nuclear reactors [Melese and Katz, 1984; Johnson and Sato, HTR2010; McEligot and Johnson, NERS 2017] for which such data were not readily available. This simple geometry generates interesting streamwise behaviors, particularly for transitional and turbulent flow regimes.

The beveled entrance forms a convergence which causes the inlet flow to accelerate as it approaches the wide rectangular duct of constant cross section. A boundary layer develops along the surface of the bevel. In his Sc.D. thesis, Launder [p. 45, Mech. Eng., MIT 1964] showed that such boundary layers, if turbulent, will revert to laminar if an associated acceleration parameter $K_V = (\nu/U_\infty^2)\, dU_\infty/dx$ persists at greater than about 2×10^{-6}. So the flow entering the duct can be expected to be partially developed and may be laminar, transitional or turbulent, depending on the generated parameters and the flow quantities.

Downstream of the edge at the intersection of the bevel surface and the rectangular duct, a separation bubble typically forms. The free shear layer between the recirculating shear flow and the core flow headed downstream would form a mean velocity profile with an inflection which is inherently unstable [Sec. XVI.b.5, Schlichting 6, 1968]. So, if the incoming core flow is laminar, it may or may not undergo a transition to turbulent before attaching to the wall of the rectangular duct. Thus, it is not clear what the effective "initial" conditions are for the downstream flow in the duct. The present measurements may give some insight into this uncertainty for flows based on Reynolds numbers ($Re_{Dh} = V_b D_h/\nu$) between about 1000 and 10,000 for a pair of plate spacings.

The discussions above consider the two-dimensional aspects of the flow in accordance with the imposed boundary conditions. However, in the experiment, curvature of the mean streamlines of the flow from the upstream plenum into the converging entry and again from the bevel boundary layer into the rectangular duct could be expected to induce three-dimensional Görtler vortices [Görtler, Göttingen 1940; Blackwelder, Phys. Fl. 1983; Finnis and Brown, J. Turbo. 1989]. These vortices could propagate into the shear layer of the separation bubble at the

beginning of the duct. If so, the effective initial conditions for the rectangular duct would be three-dimensional with imbedded streamwise vortices adding spatial fluctuations to calculations of two-dimensional mean values. While more detailed measurements or direct numerical simulations are required to examine these speculative aspects, the present data *may* give insight into whether they are consistent or not.

The air employed is considered to be non-compressed, to have constant Newtonian properties and to be flowing steadily in the mean. The containing surfaces are treated as hydraulically-smooth planes. For clarity, we will try to refer to the converging upstream geometry as the "inlet" in the rest of this report. The term "entry" will then be used to describe the hydraulic entry or developing flow region within the rectangular duct of constant cross section, beginning at the end of the bevels of the converging inlet. All the data presented are in the constant cross section region of the test section.

Lacking the ability to measure internal velocity profiles in the thin duct, for the most part we present the current experimental results in terms of the *local or pointwise apparent friction factor,* f_{app}, based on the local apparent wall shear stress, $\tau_{W,app} = (-D_h/4)\, d(P + (G^2/\rho))/dx$, from a one-dimensional momentum equation. Thus, $f_{app} = (-2\rho/G^2)\,(D_h/4)\, d(P + (G^2/\rho))/dx$ and the momentum term disappears for the current duct with a constant cross-section and incompressible flow. This pointwise definition differs from that of Kays [text 1966] and various other authors who use an overall apparent friction factor based on the pressure difference from the inlet at x = 0 to a downstream value of x. In the fully-developed region downstream f_{app} is equal to the local friction factor based on measured wall shear stress, $f_S = 2\,\tau_W/(\rho V_b^2)$, since the two-dimensional streamwise momentum flux distribution is not varying there. However, as shown by Schade and McEligot [IJHMT 1971] in the constant property section of their Table 3, in the hydraulic entry of a wide rectangular duct f_{app} is larger than f_S (their Table 2 evidently has a typographical error in the comparable section). This local $f_{app}\{x\}$ is typically employed for introductory treatments of internal compressible flows, e.g., Shapiro, p. 164 [text 1953].

Beyond engineering textbooks (e.g., Schlichting 6 [1968], Kays [1966], White 2 [1991]) and handbooks (e.g., Johnson [1998], Rohsenow and Hartnett [1973], Kakac, Shah and Aung [1987], Idelchik [1994]), flow between parallel plates has received extensive treatment in the technical literature, particularly the idealized infinitely-wide case. Reviews of the status of transition knowledge have been published by Kleiser and Zang [1991], considering numerical simulations, Zaki [FTC 2013] covering bypass transition of boundary layers, Mullin [2011] for pipe flow experiments, He and Seddighi [2013] for unsteady flows, Eckhardt et al. [Annu.Rev.F.M. 2007], Tuckerman, Chantry and Barkley [Annu.Rev.F.M. 2020], Yimprasert et al. [Exp.Fl. 2021] and Avila, Barkley and Hof [Annu.Rev.F.M. 2023] for transition in internal flows and many others. For direct comparison to the present results one is interested in streamwise pressure distributions and friction factors. Examples of pertinent studies are results from numerical analyses of laminar hydraulic entries by Schade and McEligot [IJHMT 1971], Shah and London [Adv.H.T., 1978] and Muzychka and Yovanovich [J.FluidsEng. 2009], correlations of fully-developed laminar friction factors in rectangular ducts by Kakac, Shah and Aung (their eq. 3.158 [Handbook 1987]), critical Reynolds numbers for non-circular ducts by Tosun, Uner and Ozgen [Ind.Eng.Chem.Res. 1988] and delPlace [J.Mod.Appl.Phys. 2018], direct numerical simulations for fully-developed flows between parallel plates by Kawamura and colleagues [Tsukahara et al., WCCM VI 2004, 1IFHT 2004] and for fully-developed turbulent flow in square and rectangular ducts by Ulmann et al. [JFM 2007], Vinuesa et al. [J.Turbo. 2014] and Owolabi [Ph.D. thesis 2018], channel flow experiments by Durst et al. [Exp.Fl. 1996], Hashimoto et al. [THMT 2009], Seki and Matsubara [Phys.Fl. 2012], Watanabe et al. [9ICFD Sendai 2012], Miyazaki [MS thesis Shinshu 2014], Matsubara et al. [IJHFF 2016] and Sano and Takei [Nat.Phys. 2016], extension of the Blasius correlation for fully-developed turbulent pipe flow to non-circular ducts [Blasius, 1913; Kays eq. 6-44, 1966; Schlichting 6 eq. 20.5, 1968; Bejan pg. 259, 1984] and correlations of their own developed turbulent channel flow experiments by Beavers, Sparrow and Lloyd [J.BasicEng, 1971] and by Zanoun, Nagib and Durst [Fl.Dyn.Res. 2009]. For planar channels, most theoretical studies of stability and transition have concentrated on the fully developed conditions downstream, ignoring the entry region where transition may be initiated; as will be seen in the present results, for most of the transitioning cases the transition would have started upstream before a fully-developed laminar condition would have been reached.

In transitional pipe flow, Wygnanski and Champagne [1973] observed structures called puffs and slugs. A structure comparable to the puff was found by Tsukahara et al. [2005] with DNS for a fully developed, low-Reynolds-number channel flow; based on the appearance they labeled it a turbulent stripe pattern. Fukudome and Iida [2012] have also examined stripe patterns with DNS. To verify the stripe pattern experimentally, Hashimoto et al. [2009] performed flow visualization at $(x/s) \approx 380$ in a planar channel with a turbulence grid in its entrance (x = streamwise coordinate and s = plate spacing). At this location the critical Re_{Dh} was 2600, turbulent spots occurred at Re_{Dh} about 3200, for $3400 < Re_{Dh} < 4000$ turbulent stripes were observed and at $Re_{Dh} \approx 4800$ typical high-Re-turbulence was seen. The generation of turbulent spots and their spread in channels have been studied by Carlson, Windall and Peeters [1982], Schumacher and Eckhardt [2001] and Lagha [2007]. Direct numerical simulations of transitional flow in rectangular ducts have been conducted by Takeishi et al. [JFM 2015], Rehman et al. [ISTEGIM Erlangen 2019], Orlandi and Pirozzoli [J.Turb. 2020], Kohyama, Sano and Tsukahara [Phys.Fl. 2022]; these studies all use periodicity for their streamwise boundary conditions as in fully-developed flow (even though transitional flows often occur in developing flows).

Some studies have provided insight into entry behavior. Of course, first were the flow visualization experiments of Reynolds [1883; Jackson and Launder, Annu.Rev.F.M. 2007; Mullin, 2011] although one should probably check the studies of Leonardo da Vinci. For a circular tube, Rotta [1956] examined the streamwise evolution of transition in terms of the centerline intermittency for several different entrance configurations. He found the streamwise development to depend on Reynolds number Re and the individual entry shape.

For rectangular ducts, Beavers, Sparrow and Magnuson [IJHMT 1970a] measured laminar flow development in terms of the local pressure defects and compared to available analytic predictions. Beavers, Sparrow and Magnuson [IJHMT 1970b] also conducted experiments on the effects of twelve inlet geometries on the minimum Reynolds number for breakdown of laminar flow (i.e., transition in terms of the local apparent friction factor which is based on the local streamwise pressure gradient and a one-dimensional streamwise momentum equation); they found a range $2200 < Re_{Dh} < 3400$, in the last third of the ducts. Of particular

interest is their observation that, for their rounded converging inlet, upstream disturbances had no significant effect on the transition Re_{Dh}. Ghajar and Madon [1992] examined laminar entry flow and downstream transition ($x/D > 309$) with pressure drop measurements for three different inlet configurations. In preliminary studies Durst et al. [1998] measured centerline fluctuations at $(x/s) \approx 80$ in a rectangular channel to determine entry configurations (trips) to obtain fully-turbulent flow by that location. With a curvilinear converging entry and no trip, there was apparent transition behavior there for a range $2000 < (U_{cl}s/\nu) < 10^4$. Zanoun, Kito and Egbers [J.FluidsEng. 2009] presented some channel centerplane data obtained by Fischer [Ph.D. thesis Erlangen 1999] and demonstrated the effects of inlet trips on transition (defined by an increasing turbulence intensity) and the location for developed turbulence (identified by constant values of all statistical moments). With a model of a gas turbine passage between blades, Simon and colleagues [Qui and Simon, ASME paper 97-GT-455; Jiang and Simon, J.Thermphy.HeatTrans. 2005] have conducted experiments with some of the same features as expected in the present one: convergence to a throat, a separation bubble with reattachment leading to a laminar, transitional and/or turbulent wall boundary layer --- depending on the inlet turbulence, the streamwise pressure gradient and the Reynolds number --- with the flow exiting in a laminar, transitional or turbulent state.

Useful insight into the difficulties of predicting transitional (and turbulent) flow by CFD techniques is provided by the compendium of Launder and Sandham [2002]. Although turbulence models have been attempted since the 1960s [Donaldson, 1969], development of CFD techniques for transition continues [Pacciani et al., 2009; Rehman et al., ISTEGIM Erlangen 2019]. The state-of-the-art has been summarized well by Savill [1993, 2002a,b] and has been updated in various numerical studies (e.g., Lardeau, Li and Leschziner [2007], Walters and Cokljat [2008], Turner and Prosser [2009], etc.). Using CFD with a transition model by Menter et al. [2004], Abraham and colleagues [2008, 2009, 2011] studied the effects of inlet velocity profile and turbulence intensity on flow development in a circular tube and in a planar channel plus fully-developed flow in transition regions. Several types of predictive approaches have been tried with varying success, although their abilities may be accidental artifacts of the models employed [Walters and Cokljat, 2008]. Savill [1993] found no model performed satisfactorily over a wide range of conditions, including freestream turbulence and streamwise pressure

gradients. A weakness of many current systems code treatments is that they assume fully-established flow in any channels and take the transition Reynolds number as $Re_{Dh} = 2300$ exactly. For channel entries the flow regime and flow development are not well known; the transition Reynolds number and transition development are uncertain.

In light of the above introductory comments, we take our *primary objective* as obtaining insight into the evolutions of flow regimes occurring in the rectangular duct after the present converging inlet. Of particular interest are indications of the apparent flow regimes in the hydraulic entry, the resulting apparent friction factors and non-dimensional pressure gradients downstream, the dependences of the local apparent friction factors in the hydraulic entry on pertinent streamwise coordinates, the variations of the onset of transition and of the locations where constant friction factors are attained (if beyond transition onset, we call this location "developed onset" marking the approximate beginning of fully-turbulent apparent wall friction) and whether or not fully-developed laminar flow is reached before beginning transition. With the local experimental results available, a *secondary objective* --- to assess design-style CFD predictions from a popular turbulence model --- is also attacked.

Following this Introduction, Section 2 explains the experimental apparatus and procedures, ranges of some variables, flow acceleration in the converging inlet and estimated experimental uncertainties. The local measurements of the streamwise pressure gradients --- from which the other results are deduced --- are presented in Section 3. Averaged values of $f_{app,ds}$ and $(-K_{p,ds})$ are given in Section 4 for the downstream half of the test section. Section 5 provides local results for the hydraulic entry development in comparison to the laminar predictions of Schade and McEligot [IJHMT 1971] and, where appropriate, to k-ε predictions, comparisons of various normalized apparent friction factors in terms of streamwise Reynolds number and demonstrations of the locations of transition onset and developed onset relative to an idealized laminar entry length and to the test section length. Some concluding remarks are summarized in Section 6 along with discussion of similarities to the DNS of bypass transition by Nolan and Zaki [JFM 2013].

2. Experiment

2.1. Apparatus and procedures

Air flow pressure loss experiments were conducted to quantify apparent wall friction and pressure loss in a wide rectangular channel with a beveled inlet. An overview of the vertical apparatus is shown in Figure 1(a). The present test section is in the region labeled "channel." Flows in the experiments were varied from laminar to turbulent regimes. Figure 1(b) is an isometric view of the channel wall plates and Figure 1(c) provides a fabrication drawing of the side with the holes for the pressure taps [Tew, e-mail 27 May 2023].

Air flow is provided by a blower on the inlet side. The air enters an inlet plenum upstream of the test section. Plumbing to the inlet plenum is nominal pipe size (NPS) of 3 inches, Schedule 40 having a design inside diameter of 3.068 in. ≈ 77.93 mm, preceded by a 2 inch NPS, Schedule 40 section (ID = 2.067 in. ≈ 52.50 mm) [Tew, e-mail 4 May 2023]. The former is approximately 1300 mm long and the latter is about 2100 mm. Thus, a jet of initial diameter about 77.93 mm enters the inlet plenum which is about 350.5 mm square and 609.6 mm. long. For the conditions of the present experiments the flow in the inlet pipe has $Re_{pipe} >$ ~ 2780 so this flow is likely turbulent. Even if the flow in the pipe is not fully-turbulent, its jet can be expected to become turbulent at these Reynolds numbers (e.g., Birkhoff and Zarantonello, sec. XIV.10 [text 1957]; Boguslawski and Popiel [JFM 1979]). In order to avoid a significant velocity variation across the entrance to the duct due to a jet on the centerline of the plenum, a "dispersing plate" is installed downstream of the inlet pipe based on flow visualization and computational fluid mechanics studies by Tew [MS thesis, ISU 2013]. The plate is a circular disc 152 mm in diameter located 32 mm downstream from the pipe exit. (No honeycomb or perforated plate is employed.) With this flow conditioning, the spanwise variation of mean velocity across the duct entrance was predicted to be +/- 1.4 per cent or less except at the edge boundary layers. In the flow visualization the flow approaching the duct entrance appears to be turbulent. The outlet plenum is identical to the inlet plenum except that it does not contain a dispersing plate.

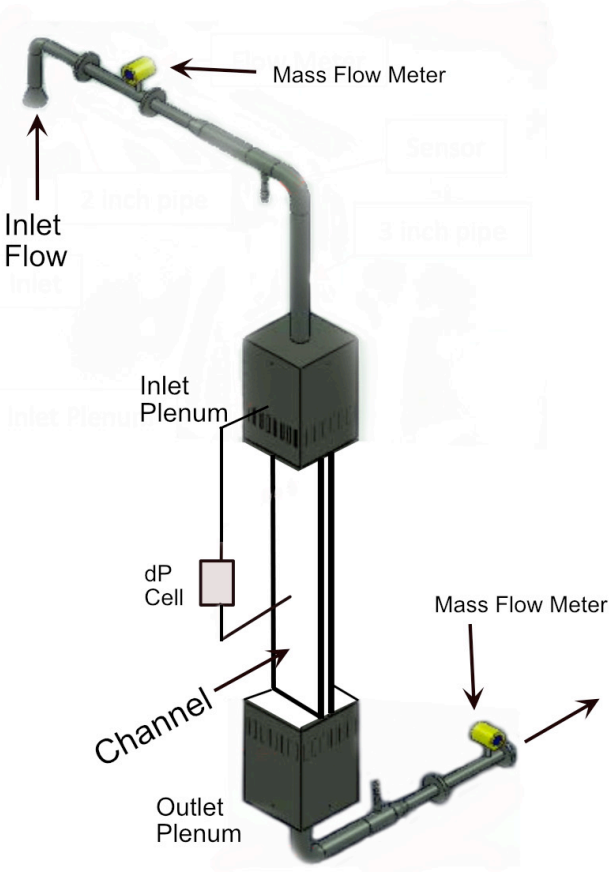

Fig. 1(a). Schematic diagram of experimental apparatus. Part of the channel serves as the test section for the present study.

The test section channel walls are constructed from two cast aluminum (Alumax Mic-6) plates, with dimensions of 1.980 m by 0.360 m, that are machined and ground to within a flatness tolerance of 0.127 mm over the length of the plates. Plate thickness is 31.75 mm (with narrow 50.80 mm thick sections at the edges). The gap between the two plates is set by clamping sets of shims between the channel wall plates at the edges. The two gap widths used in

the experiments had spacings s of three and four mm (nominal). The plate on one side has a series of evenly spaced pressure tap holes at 25.4 mm; the orifices of these pressure taps are counterbored to 3/32 in. diameter (~ 2.58 mm). The exit path consists of a beveled expansion and beveled contraction (with the same dimensions as the beveled inlet) followed by a short rectangular section and then the outlet plenum; this geometry is provided for alternate experiments which are not treated in the present study.

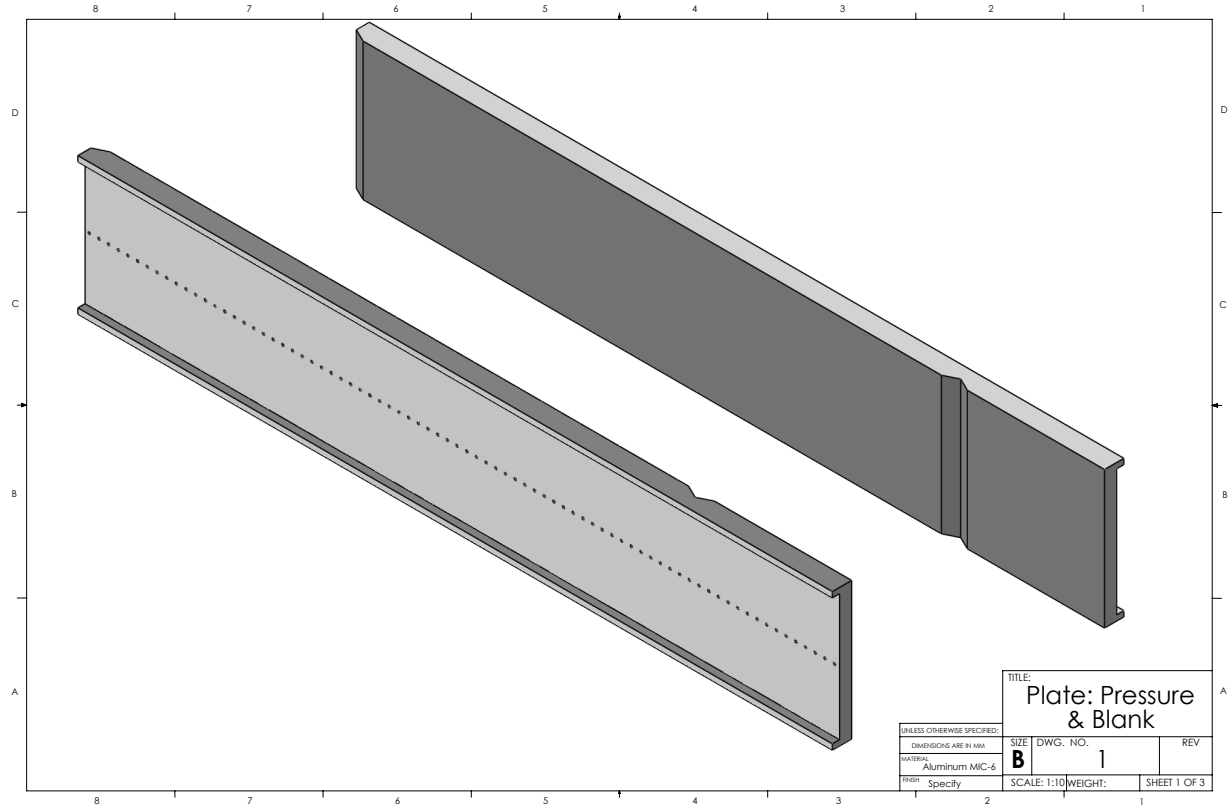

Fig. 1(b). Isometric sketch of plates for the wide walls of the channel. Air flow through the channel is from left to right [Tew, e-mail 27 May 2023].

Instrumentation consisted of two identical mass flow meters (Model ST75V by Fluid Components International LLC of San Marcos, Calif.), one placed upstream of the inlet plenum and one downstream of the outlet plenum, upstream and downstream humidity/temperature/ barometric pressure probes (Model HX85BA from Omega Engineering, Inc. of Norwalk, Conn.) and a digital manometer (Model HH35.31DLC1.0 by Huber Instrumente, Reigoldswil, Switzerland) for differential pressure measurements.

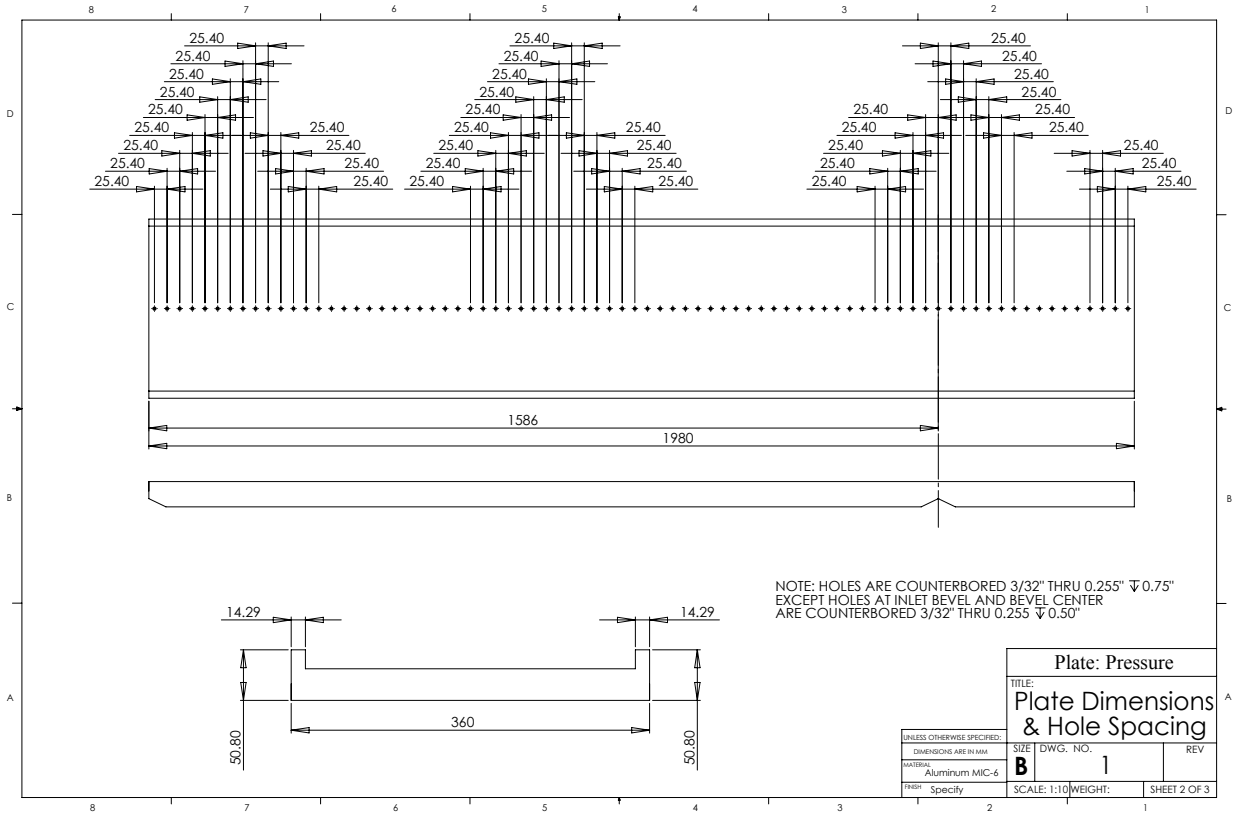

Fig. 1(c). Fabrication drawing of channel wall plate which has counterbored holes for measurement of streamwise pressure distribution [Tew, e-mail 27 May 2023].

For the *pressure drop* in the downstream region expected to have fully-developed flow, differential pressure measurements were taken directly between $x \approx 0.621$ m and $x \approx 1.408$ or 1.535 m, where $x = 0$ is at the upstream end of the converging inlet (i.e., upstream edge of the aluminum plate). To obtain the streamwise pressure distribution $P\{x\}$ in the hydraulic entry of the rectangular duct, *differential pressure measurements* are taken with one leg of the digital manometer remaining attached to the inlet plenum and the other attached to the desired individual pressure tap. Once mass flow rate has been set by adjusting the upstream blower flow rate, differential pressure is measured sequentially in the downstream direction between the plenum and each of the individual pressure taps. The measurements are then repeated in reverse order. The gage *pressure in the inlet plenum* was measured relative to the laboratory atmospheric pressure also with the digital manometer. The absolute atmospheric pressure was estimated via the INL website of the U.S. National Oceanic and Atmospheric Administration (www.noaa.in.gov/mvp/iviz/) to within about seventy Pa [McCreery, e-mail 19 Apr 2023].

Measurements are recorded using LabView computer software for later analysis. Further details are available in the report by Williams [2015].

2.2. Ranges of variables

As mentioned, two values of the plate spacing were employed in the experiments, s = 3.030 +/- 0.14 and 4.077 +/- 0.14 mm, referred to as three and four mm, respectively. In addition to the plate spacing, the inlet flow behavior can be expected to be affected geometrically by the duct width and by the bevel angle and one leg (or any two legs) of the triangle defining the bevels forming the inlet. The width of the four mm test section was 347.3 mm, giving the non-dimensional width or aspect ratio as $(W/s) \approx 85.19$, and hydraulic diameter was $D_h \approx 8.059$ mm. Its length between the end of the inlet bevel and the beginning of the exit bevel was 1.5174 m or $(L/s) \approx 372.2$, i.e., the length of the constant cross section. The hydraulic diameter of the three mm version was 6.008 mm; its width and length were the same as the four mm duct, giving $(W/s) \approx 114.6$ and $(L/s) \approx 500.8$, accordingly. The bevel leg dimensions were 34.29 mm in the streamwise direction (x) and 16.61 mm transverse (y) giving an angle with the centerplane of 25.85 degrees [Tew, e-mail 27 May 2023]. The convergence ratio of the beveled entry can be described as $(s + 2\Delta y_{TL})/s$ where Δy_{TL} is the length of the transverse leg; thus, this convergence ratio is 11.96 for the three mm test section and 9.15 for the four mm one.

Two types of measurements were employed: (1) to obtain data for developed flow an overall pressure drop was measured over approximately the last sixty per cent of the measurement region, from $x \approx 0.621$ m to $x \approx 1.408$ or 1.535 m and (2) to examine flow development including the hydraulic entry region downstream of the beveled inlet, more detailed pressure distributions were determined at 25.4 mm intervals from $x \approx 0.0112$ m to $x \approx 1.535$ m (the inlet bevel ends at 0.03125 m). The downstream measurements covered the ranges $\sim 997 < Re_{Dh} < \sim 8870$ for 34 three mm cases and $\sim 993 < Re_{Dh} < \sim 10{,}020$ for 37 four mm ones. For the detailed series with the three mm test section, nine runs were conducted across the range $\sim 980 < Re_{Dh} < \sim 8890$. The range was $\sim 1000 < Re_{Dh} < \sim 9920$ for the fifteen runs in the four mm series.

To estimate the magnitude of the acceleration parameter K_V in the converging inlet formed by the bevels, we assume the wide rectangular ducts are infinitely wide for convenience. With this assumption and the one-dimensional continuity equation, the local $Re_{Dh}\{x\}$ in the converging entry can be shown to be a constant value. This value then can be evaluated at the downstream end of the inlet bevel where it is equal to the duct value, i.e.,

$$Re_{Dh,inlet}\{x\} = Re_{Dh}\{x\text{-}x_{bevel\,=\,0}\} = Re_{Dh,duct} = \text{constant}$$

Also with this assumption, $D_h\{x\} = 2\ s\{x\}$. Within the inlet the spacing between the bevel surfaces can be described as $s\{x\} = s_{duct} + 2\ y\{x\}$ where $y\{x\}$ is the one-sided expansion from the duct wall and s_{duct} temporarily identifies the downstream duct spacing. From the definition of Re_{Dh}, the local bulk velocity in the inlet may be written as

$$V_b\{x\} = (\nu\ Re_{Dh}\{x\}/\ D_h\{x\}) = \nu\ Re_{Dh,duct}/(2\ s\{x\})$$

so the definition of K_V gives $K_V\{x\} = (-2/Re_{Dh,duct})\ ds\{x\}/dx$ there. For the plane surfaces of the bevels, the slope is constant at $(dy/dx) = (-1)\ \Delta y_{TL}/\Delta x_{BL}$ where Δx_{BL} is the streamwise length of the bevel. Thus, for this idealized geometry

$$K_V\{x\} = (4/Re_{Dh,duct})\ (\Delta y_{TL}/\Delta x_{BL})$$

For the present dimensions this relation can be evaluated as $K_V\{x\} \approx 1.938/Re_{Dh,duct}$ and the resulting range of entry acceleration parameters for the experiments is $2.0 \times 10^{-3} > K_V > 1.9 \times 10^{-4}$, approximately. These values are orders-of-magnitude greater than the laminarizing thresholds of Launder [Mech. Eng., MIT 1964], Mayle [J. Turbo 1991] and others.

For the rest of this paper, the nomenclature "s" and "Re_{Dh}" will refer to their constant values in the duct between the beveled inlet and exit.

2.3. Experimental uncertainty estimates

The key measurements of the present experiment are streamwise pressure distribution, air mass flow rate, geometric dimensions and --- for determining properties --- air temperature. These quantities are employed to deduce results such as apparent friction factor, pressure gradient parameter, Reynolds numbers and non-dimensional locations.

Typical variation of the absolute air temperature during a run measuring P{x} was about 0.7 per cent or less, leading to a 0.7 per cent contribution in the random uncertainty of the density and about 0.5 per cent in dynamic viscosity. For the downstream pressure drops, the air temperature was measured for each case so this uncertainty did not enter the consequent results. The vendor of the airflow temperature probes lists +/- 0.5 C as their accuracy; at 20 C this value is about 0.2 per cent of the absolute temperature.

The effects of atmospheric water vapor on density and viscosity were estimated to be negligible at the laboratory temperatures and humidities of the present experiment so dry air properties were employed in data reduction. As noted, the laboratory atmospheric pressure was estimated within 70 Pa. With the laboratory located at 4477 ft ASL ≈ 1365 m ASL, a typical atmospheric pressure is about 0.86 atm ≈ 87 kPa so the uncertainty in laboratory absolute pressure was 0.08 per cent or less. For the range of the present experiments the air compressibility Z = PV/(RT) was 0.9997-0.9998 [Hilsenrath et al., NBS 564, 1955], within 0.03 per cent of the perfect gas approximation which was used to calculate the air density. For the downstream friction factor the random uncertainty in density is about 0.2 per cent.

To estimate the absolute viscosity we used a version of the Sutherland formula [Phil. Mag. 1893]

$$(\mu/\mu_0) \approx (T/T_0)^{1/2} (1 + S/T_0) / (1 + S/T)$$

(his eqn. (4), page 513) where S is the Sutherland constant (Sutherland called it C as in constant). Rather than forming and solving a full mathematical kinetic theory for the viscosity, Sutherland

employed simplifications which led to his eqn. (4) and then evaluated S primarily by comparison to the experimental results provided by Holman [Phil. Mag. 1886] for the range 0 ~/< T ~/< 124 C. He concluded that a mean value of S = 113 K gave results "within the limits of experimental error." White [text 1991] recommends T_0 = 273 K, $\mu_0 = 1.716 \times 10^{-5}$ Nsec/m^2 and S = 111 K. Schlichting [1968] cites van Driest [NACA TN 2597, 1952] as assuming S = 110 K. Flügge-Lotz and Blottner [AD 273 983, 1962] employed S = 216 R ≈ 120 K and S = 198.6 R ≈ 110.33 for comparisons with other studies. They indicate that "newer reports" favor S = 198.6 R ≈ 110.33 K. A NASA Glenn Research Center website recently recommended $\mu_0 = 3.62 \times 10^{-7}$ lbf-sec/ft^2 at T_0 = 518.7 R ≈ 288.17 K with S = 198.72 R ≈ 110.4 K [www.grc.nasa.gov/www/BGH/viscosity.html accessed 12 May 2023]. Gottlieb and Ritzel [Suffield DRL TN, 1979] fit air viscosity data with a coefficient $a_0 \approx 1.47 \times 10^{-6}$ kg/(m-sec-$K^{1/2}$ and S = 113 K. Hilsenrath et al. [NBS 564, 1955] calculated air viscosity from an empirical formula which they fitted to existing experimental data (twenty separate investigations) yielding

$$\mu \text{ (poise = gm/(sec-cm))} \approx 145.8 \times 10^{-7} \, T^{3/2}/(T + 110.4)$$

(for tabulating they listed (μ/μ_0) where $\mu_0 = 1716 \times 10^{-7}$ poise or gm/(sec-cm) or 6.178×10^{-2} kg/(hr-m)). They claimed "reliability" of their viscosities is within two per cent. However, their Figure 2e shows the difference between their tabulated values and the data as mostly being less than one per cent within the temperature range of our present data. Thus, the empirical relation by Hilsenrath et al. can probably be considered to be a good representation of the viscosity data. While the various studies present ranges of values for the constants involved in the correlations of viscosity, at a laboratory temperature of 20 C the effect of the range of Sutherland constants is only about +/- 1/2 per cent, i.e., the variation of the term (T + S). For the downstream measurements the random uncertainty in viscosity can be taken as about this one per cent.

For the present measurements we used

$$\mu \text{ (kg/(sec-m) = Pa-sec)} \approx 0.0000014592\ T^{3/2} / (109.1 + T)$$

taken from a NASA Glenn Research Center website [McCreery e-mail 11 May 2023] with T in degrees K. At 290 K this relation is approximately 0.4 per cent higher than the value given by Hilsenrath et al. This difference could be considered a systematic uncertainty or an outright bias; if treated as a systematic uncertainty, the total uncertainty would become about 1.1 per cent.

The specifications of "accuracy" for the digital manometer are 0.05 per cent of full scale and 0.1 per cent of reading (but not less than 0.03 per cent of full scale). For the instrument measuring range these values indicate a random uncertainty of about 0.6 mm H_2O for direct measurements of pressure drop for the present experiment. For the downstream data with four mm spacing, resulting random uncertainties in the direct pressure gradients were about 8.1, 4.7, 1.7 and 0.7 per cent at $Re_{Dh} \approx 3090$, 3920, 5960 and 9920, respectively. With the three mm spacing, pressure drops were greater at a given Reynolds number, giving lower comparable uncertainties in pressure gradients of about 3.1 and 0.3 per cent at $Re_{Dh} \approx 2910$ and 8890, respectively.

It is estimated that the uncertainties in positions fabricated with the numerically controlled machinery employed would be about 0.0254 mm (~ 0.001 inch). Therefore the uncertainty in dx when deducing the pressure gradient dP/dx would be 0.14 per cent or less (aka negligible). For the downstream data Δx would have an uncertainty of 0.005 per cent.

While the mass flowmeter specifications claim an "accuracy" of one per cent of reading and 0.5 per cent of full scale, we estimated the random mass flow rate uncertainty as about two per cent of reading based on observations of the variability of the upstream and downstream flowmeters during individual runs.

Alcoa Mill Products describes the tolerances on MIC6 precision machined cast aluminum plate (used for the test section) as "gauge - plus/minus .005" (.127 mm), flatness - .250 to .625" .015" (.381 mm), .750" and over .005" (.127 mm)" and "finish - two sides machined smoother

than a 20 microinch or 0.50 micron surface. . . . . Flatness is measured using a feeler gauge under a straight edge when lower surface is resting on a precision ground surface" [Williams e-mail, 25 Feb 2014]. Thus, the flatness value can be considered to be essentially a peak-to-valley measurement rather than the difference from a mean. ("Gauge" refers to the thickness of the plate.)

The plate spacing is established at the edges of the rectangular duct by the thicknesses of the "gap spacers" (shims) employed. From that value the average cross-sectional spacing s, used in calculating friction factors, pressure gradient parameters and such, is determined by the flatness across and along the duct; we estimate that a worst-case effect on this average could be about one-half the tolerance specified, i.e., +/- 0.064 mm. Measurements of the gap spacers had standard deviations of about 0.025 mm for the three mm spacing and 0.032 for the four mm case; for experimental uncertainty with "20:1 odds" we select twice these values. The local spacing is given by the thickness of the gap spacers plus any "non-flatness" of each of the two plates. Thus for the four mm spacing we estimate a random uncertainty for the average spacing to be about 0.11 mm or 2.7 per cent. For the three mm case the comparable uncertainty is 3.4 per cent. Random uncertainty in width W is about 0.1 mm or better, giving 0.03 per cent or less.

In terms of the measured quantities, the apparent friction factor can be calculated as

$$f_{app} = \rho\, s^3\, W^2\, (-dP/dx) / [m^2\, (1 + [s/W])\,]$$

For local comparisons between results at the same location in the same test section, the errors in spacing will also be the same so the uncertainty in spacing need not be considered; the later comparisons of downstream dP{x}/dx for the four mm test section are examples. But, for comparisons to theoretical or CFD predictions of f_{app}, the uncertainty in s^3 must be included and can be significant (likewise for comparisons between three and four mm cases). The uncertainty in s does not vary with mass flow rate m so it does not affect the shape of the downstream $f_{app}\{Re_{Dh}\}$ but is seen as an uncertainty in the level of the curve, i.e., the resulting error in friction factor is a constant as m or Re_{Dh} varies. Compared to per cent uncertainties in

s^3, m^2 and --- at low Re_{Dh} --- dP, the per cent uncertainties in W^2, (1 + [s/W]) and properties can be considered to be negligible.

The Reynolds number can be calculated as

$$Re_{Dh} = 2\ m / [\ \mu\ W\ (1 + [s/W])\ ]$$

where the mass flow rate m is the dominant uncertainty. With the contribution of the viscosity uncertainty, the random uncertainty in Re_{Dh} becomes about 2.3 per cent.

The resulting "relative" uncertainties of the downstream f_{app} for the three mm cases are approximately 5.1, 4.3 and 4.0 per cent for $Re_{Dh} \approx 2910$, 3950 and 8890, respectively; that is, the random uncertainty relative among runs with the same three mm spacing. For $Re_{Dh} \approx 4000$ and greater this relative uncertainty is dominated by the uncertainty in mass flow rate. The "absolute" uncertainty for comparisons to predictions or to other spacings for the three mm cases is about eleven per cent for Re_{Dh} greater than 3000 when the uncertainty in spacing is taken into account. Comparable results for the four mm cases are relative uncertainties of 9.1, 6.2 4.4 and 4.1 per cent for $Re_{Dh} \approx 3080$, 3920, 5960 and 9920, respectively, and absolute uncertainties of about nine per cent above $Re_{Dh} \approx 5000$. At the lower Re_{Dh} the uncertainty in pressure drop dominates the relative and absolute uncertainties in f_{ds} while at higher Re_{Dh} the mass flow rate dominates the relative uncertainty and the spacing dominates the absolute uncertainty.

However, comparisons of the data for f_{ds} deduced from P{x} to the theoretical laminar predictions in the ranges ~ 1600 < Re_{Dh} < ~ 2900 for the four mm test section agree within four per cent and for the three mm are within three per cent for ~ 980 < Re_{Dh} < ~ 1960. These levels of agreement could imply that the estimated uncertainties are overly pessimistic or that some of the errors represented by the uncertainties cancel one-another.

3. Measurements

Primary measurements during an experimental run are the streamwise pressure distribution P{x}, the air temperature for property determination and the mass flow rate. To deduce the desired local apparent friction factors, local streamwise pressure gradients were calculated from P{x}; the observed values were smoothed to counter irregular variations corresponding to the experimental uncertainties in pressure differences and spacing between pressure taps. Downstream, where the gradients are approximately constant, the gradients were smoothed somewhat by determining the values over a distance from the fourth tap upstream to the fourth tap downstream from the specified local tap. In the entry region, where there is significant variation of the gradient, the smoothing and differentiation procedures of Hershey, Zakin and Simha [I&EC Fund. 1967] were applied. Figure 2 shows typical results; in this figure the axial distance is measured from the upstream beginning of the bevel at the entry.

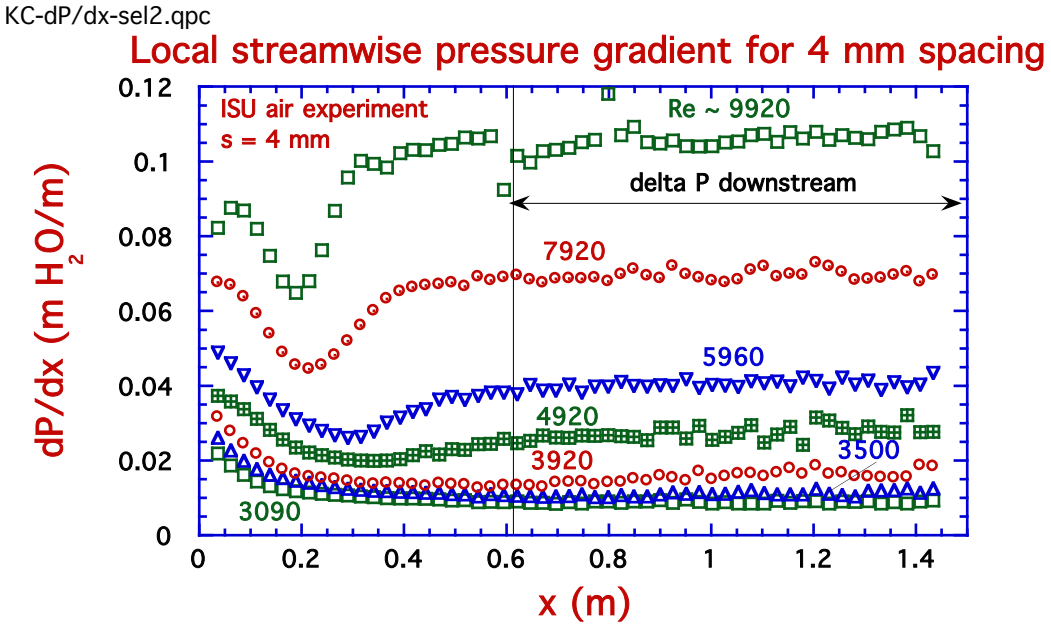

Fig. 2. Representative pressure gradient data from the series of experimental runs with plate spacing of four mm.

All the experimental runs shown have dP{x}/dx decreasing from the entry as expected for a hydraulic entry [Kays text, 1966]. The lowest run shown, at $Re_{Dh} \approx 3090$, decreases to an approximately constant value by $x \approx 0.5$ m, indicating a fully-developed flow downstream. All runs at lower Reynolds numbers, $\sim 1000 < Re_{Dh} < \sim 2940$, have approximately linear P{x} (not shown) and, therefore, constant pressure gradients for $x > \sim 0.27$ m or less and have the same shape as the run at $Re_{Dh} \approx 3090$.

The runs at higher Reynolds numbers (e.g., $Re_{Dh} \approx 3500$ and greater) have dP/dx decreasing to a minimum and then increasing. These minima occur at successively shorter streamwise distances as the Reynolds number increases. For the three highest Re_{Dh} cases shown, the dP/dx results increase to a constant value downstream, again indicating fully-developed regions --- starting about 0.8 m, 0.55 m and 0.5 m for $Re_{Dh} \approx 5960$, 7920 and 9920, respectively.

For the intermediate runs, $\sim 3500 < Re_{Dh} < 4920$, the pressure gradient is still gradually increasing at the end of the measurement region. We suspect that the downstream results represent fully-developed laminar flow, transitional flow and fully-developed turbulent flow for the low-Reynolds-number, intermediate-Reynolds-number and high-Reynolds-number groups, respectively. However, we need more evidence to confirm these suspicions quantitatively.

Also of interest is the question of how well typical computational fluid dynamics (CFD) approaches will predict these sorts of flows. A typical design approach, as by McEligot and Johnson [J.Nuc.Sci.Rad.Eng. 2017], is to select a transition Reynolds number and then, if the design Re_{Dh} is less, the turbulence model is suppressed. And if the design Re_{Dh} is greater, the turbulence model is applied for the entire field; e.g., the CFD calculations shown by McEligot and Johnson assumed fully turbulent flow for $Re_{Dh} = 2600$ and greater. The present data give an opportunity to assess this CFD approach since their wide duct geometry was comparable to our experiment (with slightly different edge conditions) .

4. Downstream results

In an attempt to obtain data for fully-developed friction factors, a series of measurements of downstream pressure drops was conducted. The downstream pressure difference was measured from a pressure tap at x ≈ 0.62 m to one near the exit of the test section (as marked on Figure 2). The downstream apparent friction factor is then calculated as

$$f_{app,ds} = (- 2\rho/G^2) (D_h/4) \Delta P/\Delta x$$

where the subscript "ds" means downstream.

Results for both spacings are presented in Figure 3, normalized by the friction factor for fully-developed laminar flow in a rectangular duct, $f_{fd,lam}$. For this study $f_{fd,lam}$ is determined from a correlation for a rectangular duct given by equation 3.158 of Kakac, Shah and Aung [Handbook, 1987]. This correlation gave $f_{fd,lam}\ Re_{Dh} = 23.6245$ for the four mm duct; this value differs from the idealized infinitely-wide channel ($f_{fd,lam}\ Re_{Dh} = 24$) by about 1.6 per cent. For the three mm duct the value is $f_{fd,lam}\ Re_{Dh} = 23.7197$ which is a difference of about 0.4 per cent from the four mm one. For comparison to turbulent predictions the correlation by Beavers, Sparrow and Lloyd [J.BasicEng. 1971], say BSL,

$$f_{fd,BSL} \approx 0.1268 / Re_{Dh}^{0.3}$$

is also plotted on the figure (normalized by $f_{fd,lam} = 23.625/Re_{Dh}$, the four mm duct value). Results for three mm spacing are represented by circles and for four mm spacing are by squares. Open symbols are from the pressure drop data measured directly between two specified downstream taps while solid symbols were calculated from the summed local pressure differences successively between x ≈ 0.62 m and x ≈ 1.41 m in the detailed series used for Figure 2.

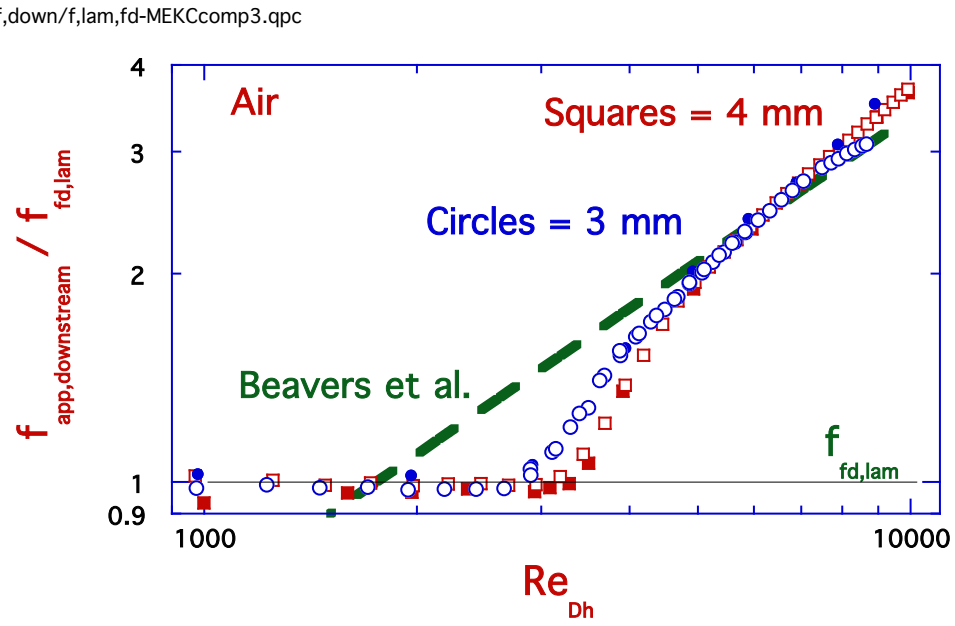

Fig. 3. Deduced apparent friction factors for defined downstream regions. Symbols explained in text.

The results agree with the laminar prediction for Re_{Dh} below about 3000; this value is in the range suggested by Beavers, Sparrow and Magnuson [IJHMT 1970b] and Kakac, Shah and Aung [Handbook 1987] for transitional Re_{Dh} for flat ducts with various entries ($2600 < Re_{Dh,tr} < 3400$). From limited water flow visualization measurements in a related geometry, McCreery et al. [NuReTH 2013] estimated that the laminar ---> turbulent transition is initiated somewhere between Re_{Dh} of 2450 and 2900; "the pressure loss measurements" of this same study "indicate that laminar flow persists to at least a Reynolds number of 2600, which is consistent with Kakac, Shah and Aung." And the present data approximately agree with the correlation of Beavers, Sparrow and Lloyd for $Re_{Dh} > \sim 5500$. (The DNS predictions for fully-developed skin friction coefficients in a duct of aspect ratio 96 by Kohyama, Sano and Tsukahara [Phys.Fl. 2022] agree with their choice of an asymptotic turbulent correlation at Re_{Dh} about 6400 as seen in their Figure 15.) The values in the range $\sim 3000 < Re_{Dh} < \sim 5500$ correspond to the runs in Figure 2 where the pressure gradients are still increasing gradually within part or all of the region between the two taps, i.e., the flow is undergoing transition at the beginning of the region or throughout it. (In the case of $Re_{Dh} \approx$ 5960 most of the increase in dP/dx occurs before the measuring region

and it appears to be constant beyond x ≈ 0.8 m or so for about 3/4 of the measuring region.) If different taps were chosen for the measuring region, the bounds determined for the apparent transition region would be expected to differ.

Closer examination shows systematic differences between the data for three and four mm spacing. Both agree with each other in the laminar and turbulent regions. But the test section with three mm spacing appears to start transition near $Re_{Dh} \approx 2700$ while for four mm it is about $Re_{Dh} \approx 3000$. From these points the two follow slightly, but discernably, different paths until approximately agreeing with the fully-developed turbulent correlation. (In the region taken as turbulent, the slope of the present data appears to be slightly greater than the BSL correlation, corresponding to the DNS predictions of Kawamura and colleagues [Tsukahara et al., WCCM VI 2004, 1IFHT 2004], e.g., see Figure 4 of M+J). In this transitional region the runs with three mm spacing have higher $f_{app,downstream}$ at a given Re_{Dh} than the four mm ones, i.e., they are closer to the turbulent correlation or, one might say, further advanced in the transition process at that Re_{Dh}. Then, for three mm $f_{app,ds}\{Re_{Dh}\}$ appears to correspond to the fully-developed turbulent region *before the first pressure tap* for Re_{Dh} greater than about 5600 while for four mm the corresponding value is $Re_{Dh} \approx 5900$. Why these values might differ will be discussed in a later section.

In a recent water experiment Yimprasert et al. [Exp.Fl. 2021] measured downstream pressure drops and conducted flow visualization in a long rectangular duct having an upstream trip wire to induce turbulence. Their aspect ratio was about 82.6 which is close to that of our four mm test section ((W/s) ≈ 83.18). They found their downstream friction factor f_{ds} began to deviate from the fully-developed laminar prediction at around $Re_{Dh} \approx 2500$ (their Figure 3). Their flow visualization implied that the flow approached fully-turbulent for $Re_{Dh} \approx 5200$; their f_{ds} merged with their asymptotic turbulent correlation at about $Re_{Dh} \approx 5000$ (our "developed onset").

As mentioned earlier in conjunction with the converging beveled inlet, to predict transition and "laminarization" many investigators have employed an acceleration parameter, K_V

= $(\nu/U_\infty^2)\, dU_\infty/dx$ or $(\nu/V_b^2)\, dV_b/dx$ [Launder, M.S. thesis 1963; Kline et al., JFM 1967; McEligot, Coon and Perkins, IJHMT 1970; Mayle, J.Turbo 1991 and others]. (An interesting overview of early studies on laminarization is provided by Launder [ScD thesis MIT 1964].) The version for a duct flow would use the definition with the local bulk velocity, $V_b\{x\}$. However, for a duct with a constant cross section and constant fluid properties as in the present experiment, the gradient dV_b/dx is zero and therefore does not help discriminate. An alternative quantity, which has also been used, is a streamwise pressure gradient parameter, $K_p = (\nu/(\rho u_\tau^3))dp/dx$ [Bankston, JHT 1970; Narasimha and Sreenivasan, Adv.Appl.Mech. 1979]. Bankston indicated that when a wall version of $-K_p$ exceeded about 0.02 reversion to a laminar flow is likely in internal heated turbulent gas flow. Narasimha and Sreenivasan noted that apparent "laminarization" can occur at $-K_p \approx 0.03$ in turbulent boundary layers. McEligot and Eckelmann [JFM 2006] observed that Spalart [JFM 1986] could simulate turbulent flow at $-K_p = 0.02$ but not at $-K_p \approx 0.025$ with his DNS program. (Additional related studies have been summarized by Narasimha and Sreenivasan, by Murphy, Chambers and McEligot [JFM 1983], by Spalart, by McEligot and Eckelmann and many others.) Therefore, it is appropriate to examine the values of K_p for the present data.

Figure 4 provides the downstream values $K_{p,ds}$ based on the pressure difference between $x \approx 0.6208$ m and 1.408 m; the subscript ds refers to this range. Again circles represent data with three mm spacing and squares are for four mm. For comparison, predictions of $K_{p,fd}$ based on friction factor relations via their definitions,

$$K_{p,fd} = (-4) / [Re_{Dh} (f_{fd}/2)^{1/2}],$$

are shown as dashed lines. The laminar line is calculated from the analytic result for an infinitely-wide parallel plate channel, $f_{fd,lam}\, Re_{Dh} = 24$ [Kays text, 1966] as an approximation and the turbulent line is from the empirical correlation of Beavers, Sparrow and Lloyd [J.BasicEng. 1971].

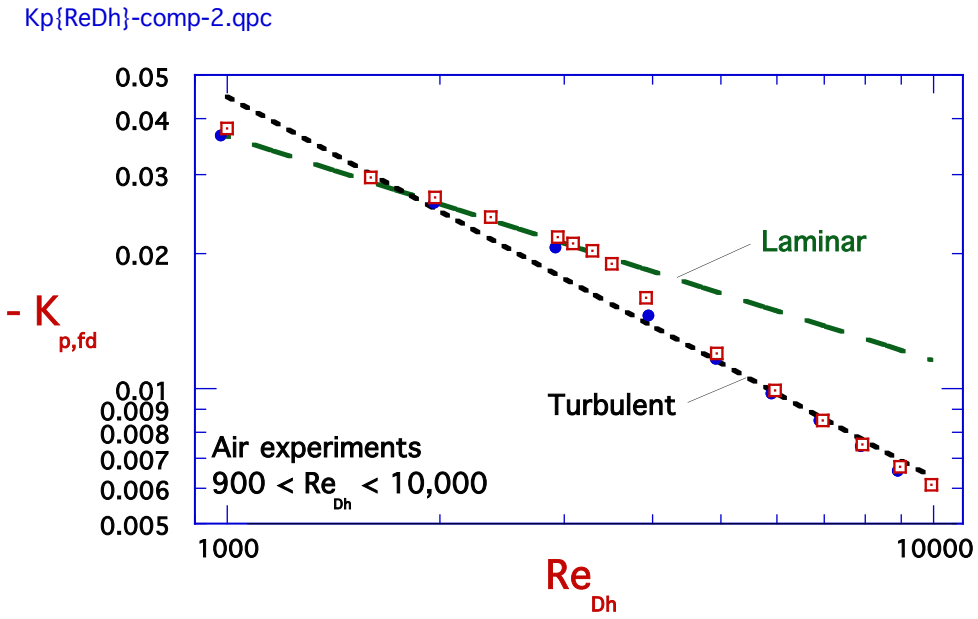

Fig. 4 Non-dimensional streamwise pressure gradient parameter, $K_p = (\nu/(\rho u_\tau^3))\, dp/dx$, for defined downstrean region from measurements, 3 mm spacing = circles, 4 mm spacing = squares.

From the f_{ds} results in Figure 3 we estimated that the downstream data for *three mm* spacing agreed with the laminar correlation of Kakac, Shah and Aung [eqn. 3.158, handbook 1987] for Re_{Dh} less than 2800, corresponding to $-K_{p,ds}$ being 0.02195 or larger. That is, for these measurements with non-dimensional length (L/s) < or ≈ 453.4 (downstream pressure tap) if $-K_{p,ds} > \sim 0.022$, the flow appeared to remain laminar. For the *four mm* duct we estimated that laminar flow apparently was retained in the downstream measurement region to $Re_{Dh} \approx 3200$. This result converts to the observation that for its length (L/s) ≈ 337.0 laminar f_{fd} values were obtained for $-K_{p,ds} > 0.021$ and larger.

In this graph of $-K_{p,ds}\{Re_{Dh}\}$ the *three mm* measurements first agree with the turbulent correlation at the data point for $Re_{Dh} \approx 4910$. Thus, for $-K_{p,ds} \approx 0.0117$ or less, developed turbulent flow appeared by (x/s) ≈ 193.6 (upstream pressure tap) or sooner. With the *four mm*

test section the corresponding values become $Re_{Dh} \approx 5960$ giving $-K_{p,ds} \approx 0.00992$ or less yielding developed turbulent flow by $(x/s) \approx 143.86$ or sooner.

5. Hydraulic entry behavior

As noted in the Introduction, an effect of the converging inlet upstream of the constant cross section duct is to accelerate the incoming flow, possibly stabilizing it. But one also expects a separation bubble to be formed downstream of the bevel's edge where the bevel wall intersects the wall of the constant cross section part; the free shear layer of the separation bubble is expected to be destabilizing. So it is not immediately clear whether to expect laminar or turbulent flow in the first part of the duct.

5.1. Comparison to idealized two-dimensional laminar entry prediction

To examine the duct hydraulic entry region data, some of the results for both three and four mm spacings are presented in Figures 5-8 using logarithmic coordinates. The ordinate gives the local apparent friction factor normalized by the appropriate fully-developed value for laminar flow; for the present data $f_{lam,fd}$ is taken from the correlation of Kakac, Shah and Aung [Handbook, 1987] evaluated at the appropriate aspect ratio (as in earlier Figure 3), i.e., $(W/s) \approx 114.6$ for three mm and ~ 85.2 for four. The abscissa is the streamwise distance from the upstream bevel's edge at the intersection between the bevel and the constant area duct non-dimensionalized by the spacing times Re_{Dh}. (i.e., $x^* = (x-x_{bevel})/(sRe_{Dh})$) The physical lengths of the test sections for all experiments are the same so, as Re_{Dh} increases, the non-dimensional test section length shortens since Re_{Dh} is in the denominator. Likewise, for equal Re_{Dh}, four mm cases appear shorter than the corresponding three mm cases because the spacing is also in the denominator. In turbulent flow, while the predicted $f_{app,fd}$ decreases as Re_{Dh} increases, the denominator $f_{lam,fd} = C/Re_{Dh}$ decreases more with Re_{Dh} so plotted values of $f_{app,fd}/f_{lam,fd}$ increase with Re_{Dh}. Downstream the three mm results show a systematic variation which could be equivalent to the change induced by a slight bowing of one wall of about sixty μm (~ 0.002 in.).

For reference purposes in these figures, the numerical predictions by Schade and McEligot [IJHMT 1971] for *laminar* entry flow in an infinitely-wide parallel plate duct with an uniform velocity profile at the inlet are provided as curves of long dashes. Also for comparison, on some figures are *turbulent* predictions by McEligot and Johnson [NERS 2017] from a popular k-ε turbulence model as a solid curve and from the turbulent correlation for fully-developed duct flow by Beavers, Sparrow and Lloyd [J.BasicEng. 1971] as thin horizontal lines. The increase of $f_{app}\{x\}$ at the end of the k-ε curve is believed to be due to upstream influence from the beveled exit of this test section. In many cases a four mm run is at approximately the same Re_{Dh} as a three mm one so they are grouped closely on the figures. The lines plotted for the Beavers, Sparrow and Lloyd correlation (BSL) have been calculated at the Re_{Dh} of the corresponding four mm run.

In the duct hydraulic entry region all the present data follow the laminar entry prediction with most appearing to be displaced somewhat in the downstream direction. Thus, we consider the duct entry flow effectively to be laminar. This downstream displacement could indicate a streamwise delay until U{y} agrees with its shape in the predictions of the idealized laminar entry treated by Schade and McEligot [IJHMT 1971]. Alternatively, this appearance might be considered as an increase in $f_{app}\{x^*\}$ due to the smaller cross section for downstream-directed flow as a consequence of separation bubbles on both walls (i.e., forming a vena contracta). Dye flow visualization by McCreery [e-mail 16 Jan 2012; NuReTH 2013; Williams, ISU rpt 2015] in a comparable 3.5 mm water channel showed a slight separation bubble of about 0.30 +/- 0.15 mm thickness downstream of the bevel edge in photos at $Re_{Dh} \approx 700$ and 1750.

Figure 5 presents data for some "low" Reynolds numbers (low in the sense of the present experiment). Shown for the three mm test section are runs at $Re_{Dh} \approx 1960$ (diamonds) and $Re_{Dh} \approx 2910$ (circles) and for four mm $Re_{Dh} \approx 2940$ (squares) and $Re_{Dh} \approx 3090$ (crossed squares). Though obscured by other data, the three mm run at $Re_{Dh} \approx 2910$ follows the trend of the laminar entry prediction to a minimum at about $x^* \approx 0.072$ and then, on average, may show a slight increase downstream that may be interpreted as the beginning of a gradual transition to

fully-turbulent flow that is not completed before the end of the test section (the downstream behavior appears better with a linear abscissa but is still confused by the downstream variation mentioned earlier). As a conclusion, this observation is considered possible but questionable. On the other hand, the fully-developed (streamwise periodic) DNS results of Kohyama, Sano and Tsukahara [Phys.Fl. 2022] for (W/s) = 96 show the possibility of developed laminar-turbulent coexisting structures evolving at this Reynolds number rather than an asymptotic turbulent state; for example, see their Figure 5c which is at Re_{Dh} approximately 3100. The other three runs shown are considered to be laminar in the duct hydraulic entry region and to remain laminar to the end of the test section based on reasonable agreement with the trends of the laminar prediction as well as our earlier Figure 3 for the downstream region. Thus, these *local* data indicate that for the three mm spacing in this test section a transition may begin near $Re_{Dh} \approx$ 2910 whereas it is above $Re_{Dh} \approx 3090$ for the four mm spacing.

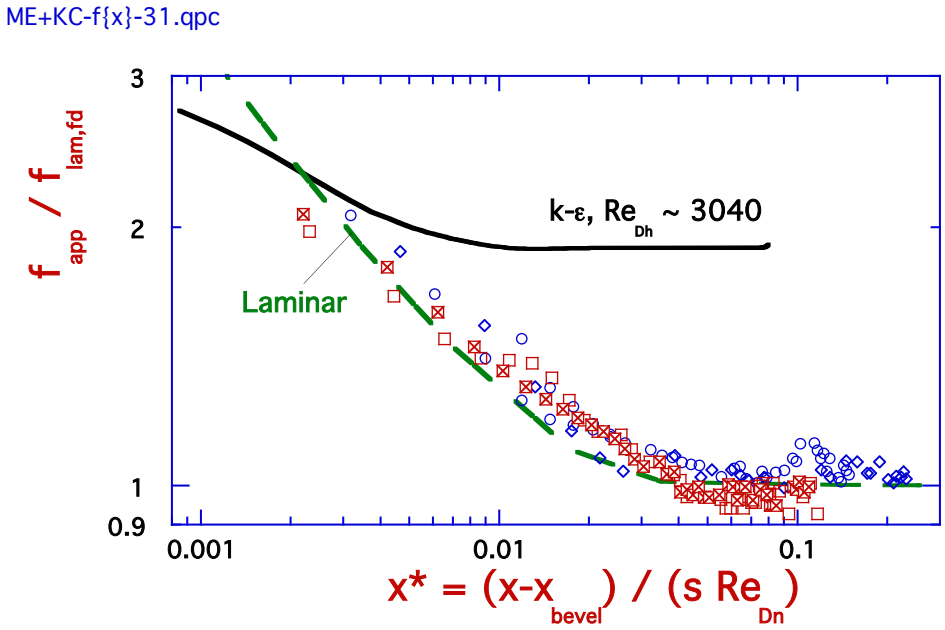

Fig. 5. Streamwise development of local apparent friction factor for some "low" Reynolds number cases. See text for explanations of symbols.

The evolution of the local apparent friction factor is shown in Figure 6 for some flows which were suspected to be "transitional flows" based on the local pressure gradients of earlier Figure 2. For clarity, only the four mm cases are displayed; the three mm detailed (local) series

has fewer cases in this category. The runs shown are at $Re_{Dh} \approx 3290$ (squares), $Re_{Dh} \approx 3500$ (diamonds), $Re_{Dh} \approx 3920$ (slashed squares), $Re_{Dh} \approx 4930$ (circles) and $Re_{Dh} \approx 5960$ (crossed squares); only the last case reaches the turbulent correlation of Beavers, Sparrow and Lloyd [J. Basic Eng. 1971] downstream.

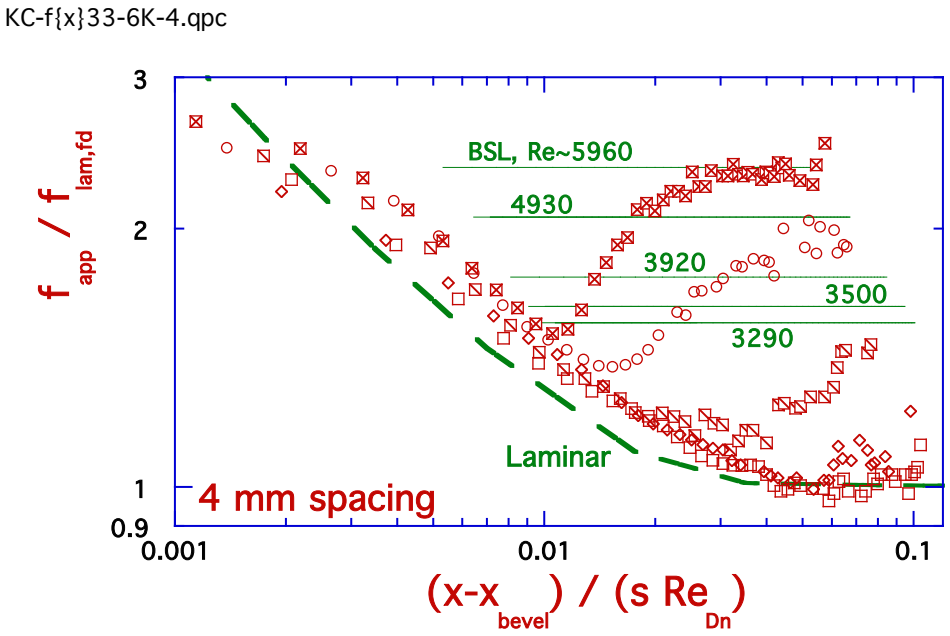

Fig. 6. Streamwise development of local apparent friction factors for four mm spacing in the Reynolds number range suspected to be "transitional flows" based on earlier observations of local streamwise pressure gradients in Figure 2. See text for explanations of symbols.

All the cases in this figure follow the laminar entrance prediction (slightly displaced downstream) to a *transition onset defined as the minimum* $f_{app}\{x\}$ [Walsh et al. JFE 2011] and then increase downstream. After the transition onset the trends are reminiscent of the intermittency factor data of Rotta [Ing.Arch. 1956] for a transitional pipe flow in a different Reynolds number range as displayed by Schlichting and Gersten in their Figure 15.3 [text 2K]. For $Re_{Dh} \approx 3290$ the transition onset is at about $((x - x_{bevel})/(s\ Re_{Dh})) \approx 0.055$ and $f_{app}\{x\}$ increases slightly going further downstream (~ six per cent by the end of the test section). As Re_{Dh} increases from case to case the apparent downstream displacement of the laminar entry curve increases slightly while transition onset moves upstream in non-dimensional distance (as well as physical distance as seen in Figure 2).

For convenience, we can refer to the location where $f_{app}\{x\}$ appears to become constant (e.g., merges with a fully-developed turbulent correlation) as the "*developed onset ;*" unfortunately, data scatter interferes with determination of precise locations. This developed onset also can serve a an approximate entry development length (based on streamwise pressure gradient) for this configuration. White (his p. 375 and Figure 5-29 [text 1991]) refers to this location as the "point of transition or fully-developed turbulent flow" and presents analyses/correlations to predict it. Simon [Qui and Simon, ASME paper 97-GT-455] and others call it "the transition end position" based on hot-wire intermittency measurements. Of these five runs, only the one at $Re_{Dh} \approx 5960$ shows a developed onset within the test section. Longer test sections would be required for the other cases ($Re_{Dh} \approx 4930$ and less) to reach a fully-developed turbulent state. In contrast, the three mm run at $Re_{Dh} \approx 4910$ does reach a developed onset before the end, as shown in the next figure.

We can hypothesize that this increasing $f_{app}\{x\}$ curve after transition onset represents a growing transitional wall boundary layer. It may be approximated as a power law of the non-dimensional streamwise distance; we call this part the "*transition growth curve*." For the cases in this figure, the slope of that curve increases as Re_{Dh} increases. As $f_{app}\{x\}$ approaches the developed onset with the BSL correlation, the slope of the data variation moderates, presumably as the boundary layer edge approaches the duct centerplane and the boundary layers on the opposing walls interact across the centerplane (e.g., see Bradshaw, Dean and McEligot [J.Fl.Eng. 1973]) while the velocity profiles begin to adjust to their fully-developed states (however, the fully-developed location is not necessarily the same for velocity profiles as for the wall shear stress). For the length of this test section, the higher Re_{Dh} runs successively come closer to reaching that fully-developed condition before the end.

Some additional intermediate Re_{Dh} runs are demonstrated in Figure 7. For the three mm test section are results for $Re_{Dh} \approx 4910$ (diamonds) and $Re_{Dh} \approx 5890$ (circles) and for four mm are $Re_{Dh} \approx 4930$ (squares) and $Re_{Dh} \approx 5960$ (crossed squares). Thus, there are two sets of paired runs (i.e., paired = two runs at about the same Re_{Dh}). For each pair the two runs follow

approximately, but not exactly, the same data locii. All the runs attain approximately constant values near the turbulent correlation of Beavers, Sparrow and Lloyd well before the end of the test section; we interpret these as fully-developed turbulent conditions. (The logarithmic abscissa makes the downstream data look worse than they are.) For each pair the transition onset is in approximately the same non-dimensional location for both runs --- and, therefore, the three mm transition onsets are physically upstream from the four mm ones. The streamwise distance to transition onset decreases as Re_{Dh} increases as in the previous figure.

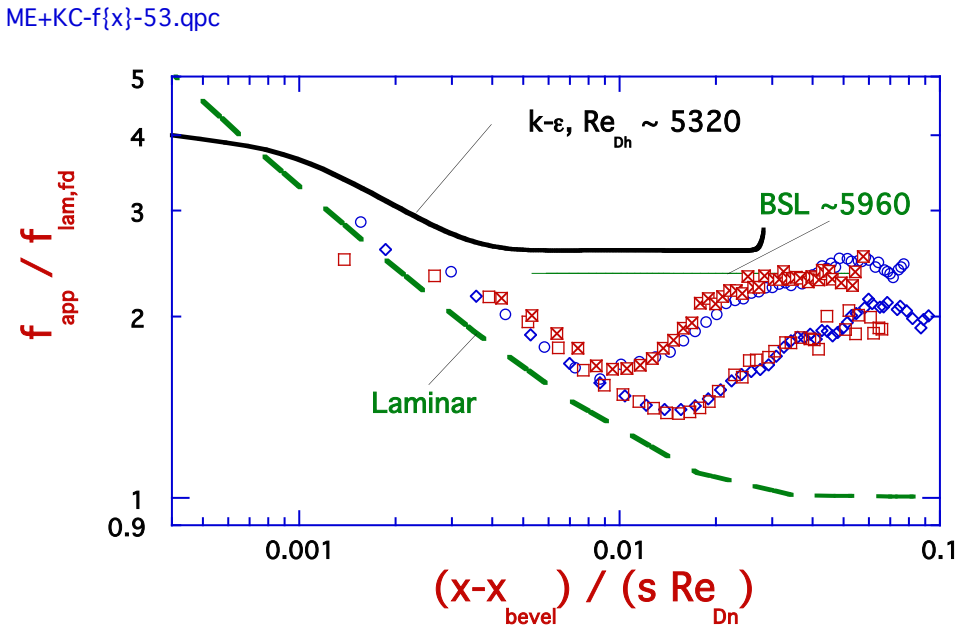

Fig. 7. Streamwise development of local apparent friction factors for some pairs of runs in the "intermediate" range. See text for explanations of symbols.

"High" Re_{Dh} data, categorized as turbulent in the downstream measurements, are provided in Figure 8. For the three mm test section are results for $Re_{Dh} \approx 6890$ (diamonds) and $Re_{Dh} \approx 7890$ (circles) and for four mm are $Re_{Dh} \approx 6960$ (squares), $Re_{Dh} \approx 7920$ (slashed squares) and $Re_{Dh} \approx 9920$ (crossed squares). In general, results continue the trends described for the previous figure. The slopes of their transition growth curves continue to increase slightly with Re_{Dh} except for the four mm run at $Re_{Dh} \approx 6960$ which has a slope a bit greater than the one at $Re_{Dh} \approx 7890$. The downstream data for the two highest Re_{Dh} are underpredicted by about four and seven per cent by the BSL turbulent correlation. In this Reynolds number range

the DNS predictions of Kawamura and colleagues [Tsukahara et al., WCCM VI 2004, 1IFHT 2004] would agree slightly better (e.g., see Figure 4 of McEligot and Johnson [NERS 2017]). For the runs at $Re_{Dh} \approx 6900$ and 7900 the three and four mm data differ from each other more in the region between transition onset and developed onset than in the previous figure; otherwise the locii of the runs in each pair are close, e.g., in the pre-transition laminar and developed turbulent regions. Some characteristics of this transition zone will be examined later in this section but first we will address comparison to turbulent CFD predictions.

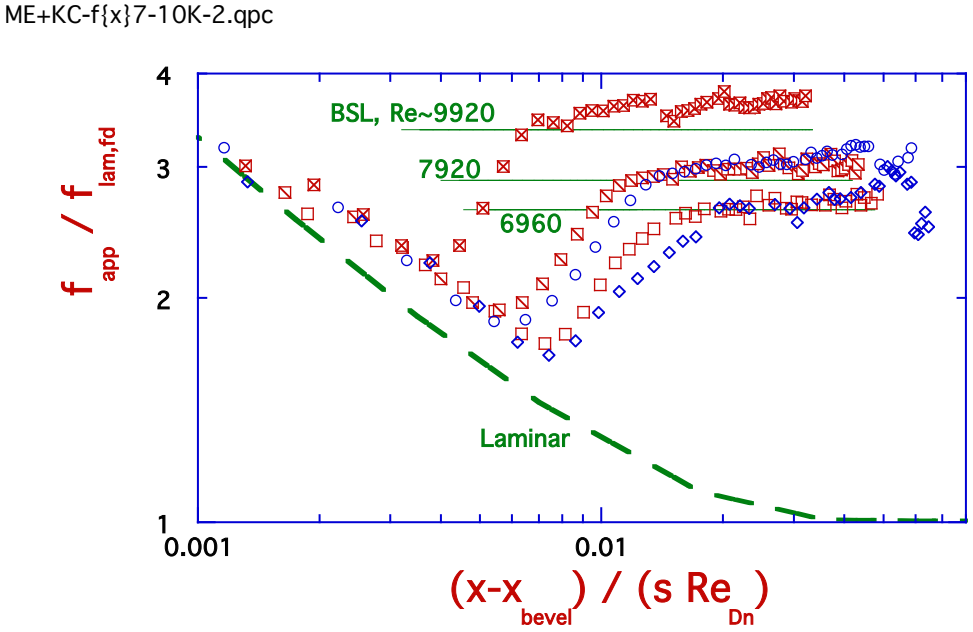

Fig. 8. Streamwise development of local apparent friction factor for some "high" Reynolds number cases. See text for explanations of symbols.

5.2. Assessment of design-style computational fluid dynamics predictions with a k-ε turbulence model

McEligot and Johnson [NERS 2017] analyzed the design-style CFD predictions of streamwise pressure distributions by Johnson for a comparable geometry [ASME paper IMECE2011-65831] to provide apparent friction factors, flow resistances and loss coefficients. The cross section consisted of wide parallel plates with a solid wall at one edge and an angled symmetry plane at the other. Inflow to this duct was via a beveled inlet. The legs of the triangle

describing the bevel were 8.3 mm normal to the duct centerplane and 17.0 mm in the streamwise direction for an angle of 26.02 degrees. The commercial code STAR-CCM+ was used for laminar and turbulent predictions for various flow ranges and plate spacings. Upstream of the beveled inlet was a plenum with uniform incoming flow which was taken to be turbulent. For flows assumed to be laminar, the turbulence model was suppressed beginning at the streamwise end of the inlet bevel. For turbulent flow the code employed the "standard k-ε two layer turbulence model with the all y^+ wall treatment." The flow was assumed to be fully-turbulent for $Re_{Dh} = 2600$ and higher based on the transition data of Patel and Head [p 186, JFM 1969] also using a wide parallel plate channel from the region of fully-developed friction factor downstream of "disturbed entry conditions."

McEligot and Johnson (M+J) presented two turbulent flows from Johnson's calculations: one with plate spacing of six mm at $Re_{Dh} \approx 3040$ and the other with s = 10 mm and $Re_{Dh} \approx 5320$. Their predicted apparent friction factor distributions are compared to some current data in our Figures 5 and 7, respectively. For both laminar and turbulent entry flows the apparent friction factors predicted by the code started above the downstream fully-developed values and decreased monotonically to their constant values of $f_{app,fd}$ downstream (their Figures 3 and 5). McEligot and Johnson also found that their *laminar* CFD entry results agreed approximately with the numerical entry predictions of Schade and McEligot [IJHMT 1971]. Figure 3 by M+J presents their laminar CFD predictions for a six mm duct; these predictions show the same trends in the immediate entry as the present four mm data in our Figure 5 but converge with the numerical predictions of Schade and McEligot at a lower value of x* than the measurements. But the shapes of our pressure gradient data for $x < \sim 0.5$ m in Figure 2 already have displayed some differences from the *turbulent* k-ε predictions of McEligot and Johnson; these differences propagate into the $f_{app}\{x\}$ data. For the k-ε results the entry predictions vary approximately as $(x-x_{bevel})^{-n}$, where $n \approx 0.2$ or 0.25, for a significant part of the developing region (also Fig. 5 by McEligot and Johnson), i.e., not as steep as the laminar entry prediction or the current data.

The k-ε predictions for $Re_{Dh} \approx 3040$ with six mm spacing over-predicted the present friction factor data for $2910 < Re_{Dh} < 3090$ by about a factor of two as seen in Figure 5. This

difference is mainly because the CFD calculations assumed the flow to be fully-turbulent whereas the experiments showed the flow to be laminar or barely transitional in this range. (If the flow was fully-turbulent, the downstream over-prediction would be reduced to about twenty per cent relative to the BSL turbulent correlation.) Examination of the present data indicates that, with six mm spacing, a flow at $Re_{Dh} \approx 3040$ would likely remain laminar in this geometry. (Figure 3 of McEligot and Johnson for laminar flow in a six mm duct at $Re_{Dh} \approx 973$ provides confidence that the code would provide reasonable predictions if the flow had been assumed to be laminar.) Since the CFD code considers the flow to be either fully-laminar (intermittency factor = 0) or fully-turbulent (intermittency factor = 1), it would also significantly over-predict $f_{app}\{x\}$ for other flows at the lower end of the transitional range such as the present data for $Re_{Dh} < \sim 4000$ in Figure 6.

The other k-ε prediction is compared to data at the upper end of our "transition range" in Figure 7. This ten mm duct flow at $Re_{Dh} \approx 5320$ is compared to pairs of data at $Re_{Dh} \approx 4900$ and 5900, a grouping that brackets its non-dimensional flow rate (Re_{Dh}). The CFD results over-predict the entry $f_{app}\{x\}$ because it is treated as a turbulent flow with a growing turbulent boundary layer rather than the laminar entry flow implied by the experiments. A crude estimate is that the flow at $Re_{Dh} \approx 5320$ should follow the laminar entry prediction until a transition onset at about $x^* \approx 0.013$ or so and then increase along its transition growth curve, between the two pairs of experimental runs, towards its fully-developed turbulent level. Since the non-dimensional length L* of the ten mm duct is shorter than for the three and four mm ducts of the experiments, it is not clear whether it would reach its fully-developed turbulent friction factor (developed onset) before the end of the test section. The k-ε calculations predict a turbulent entry length of about forty spacings but the experiments indicate it may be much longer. One ***message*** of these comparisons is that fluid dynamics engineers should exercise caution in applying results of "standard" turbulence models to duct flows in a possible transition region.

5.3. Alternate local streamwise representations

The one geometrical quantity we have varied to see its effects has been the plate spacing s. Some effects of increasing the spacing from three mm (aka 1/8th inch) to four mm have been: (1) reduction of $f_{app,ds}$ in the transition region at a given Re_{Dh}, (2) likewise a slight reduction in the range of $-K_{p,fd}$ for transition (may not be statistically significant), (3) beginning of the transition range at a higher Re_{Dh}, (4) transition onset occurs physically further downstream at a given Re_{Dh} and (5) reaching developed onset within this test section requires a higher Re_{Dh} (i.e., the entry length increases physically). Why have these transition characteristics varied?

Kähler reminded us that, for constant Re_{Dh}, the bulk velocity varies approximately inversely as the spacing [Personal communication 2014]. Thus, the unit Reynolds number Re' {= V_b/ν with units of 1/m) varies and at any streamwise distance the value of the appropriate streamwise Reynolds number varies accordingly. Increasing the velocity increases the streamwise pressure gradient needed to force the flow through the duct. For external laminar boundary layers an *increase in* a (non-dimensional) favorable *pressure gradient will move the transition onset downstream* in non-dimensional distance, e.g., Figure 9 derived from Nolan and Zaki [JFM 2013]. In this figure, long dashes present results for a favorable pressure gradient with a target λ_θ (= $(\theta^2/\nu)\, dU_\infty\{x\}/dx) \approx 0.0206$ while short dashes represent a zero pressure gradient, $\lambda_\theta \approx 0$. This decrease in spacing from four to three mm and consequent increase in velocity will provide a greater shear at the edge of the separation bubble --- and possibly induce greater turbulence there --- in the three mm case at the same Re_{Dh}. This turbulence would serve as freestream turbulence relative to the downstream wall boundary layer. For external boundary layers on a smooth flat plate we know that the position of transition onset or "critical Reynolds number" varies with the freestream turbulence [White text, Sec. 5.5, 1991; Schlichting 6, Fig. 16.16, 1968; Brandt, Schlatter and Henningson, JFM 2004]. An i*ncrease of freestream turbulence* acts to *move transition onset upstream* (e.g., compare Figures 3(a) and 3(b) by Marxen and Zaki [JFM 2019]). So these two effects of varying the plate spacing act in opposite directions and we lack information to predict which may dominate.

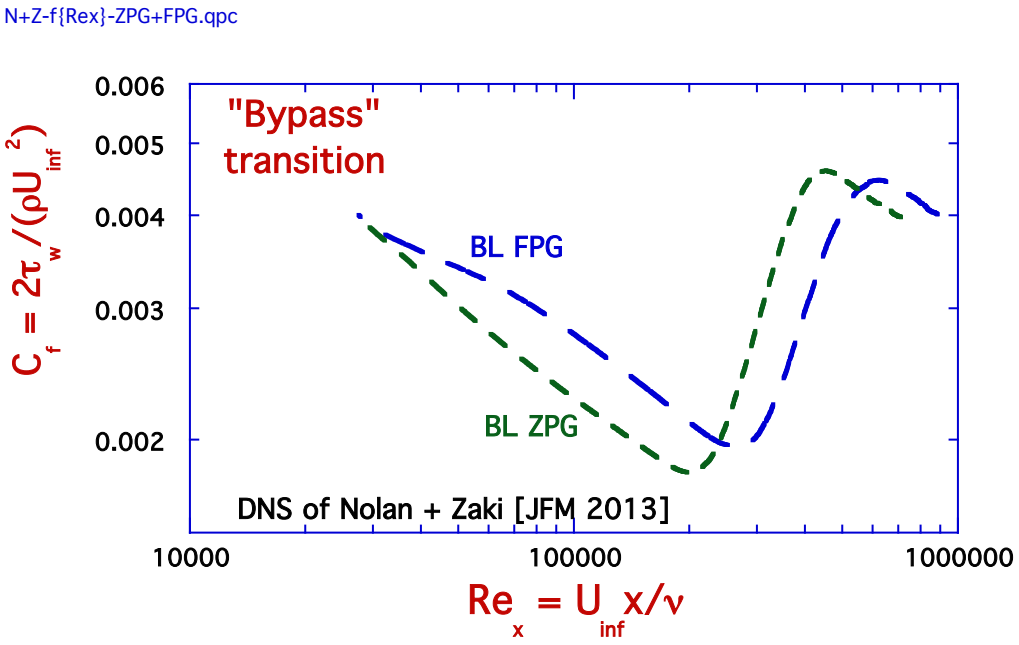

Fig. 9. Effects of a favorable streamwise pressure gradient on distribution of the skin friction coefficient in "bypass" transition (~ transition believed to be induced by freestream turbulence) of flow over a flat plate as predicted by direct numerical simulations of Nolan and Zaki [JFM 2013]. Inlet turbulence level is about three per cent for both cases.

To examine the transition process at the duct entry in terms of the streamwise Reynolds number ($Re_X = V_b x/\nu$), Figure 10 provides the streamwise distribution of the apparent friction factors for three pairs of runs in the transitional and turbulent regions. The four mm cases are shown as squares for $Re_{Dh} \approx 3920$/open, 5960/slashed and 7920/crossed while the three mm ones are $Re_{Dh} \approx 3950$ /diamonds, 5890/circles and 7890/triangles. Despite their variations in pressure gradients and suspected "freestream" (centerplane) turbulence levels, all these runs except the four mm one at $Re_{Dh} \approx 3920$, show transition onsets at Re_X slightly less than 2 x 10^5 (due to experimental scatter near the low point of that differing case it is difficult to estimate the location of its transition onset). All three pairs show some comparable behavior.

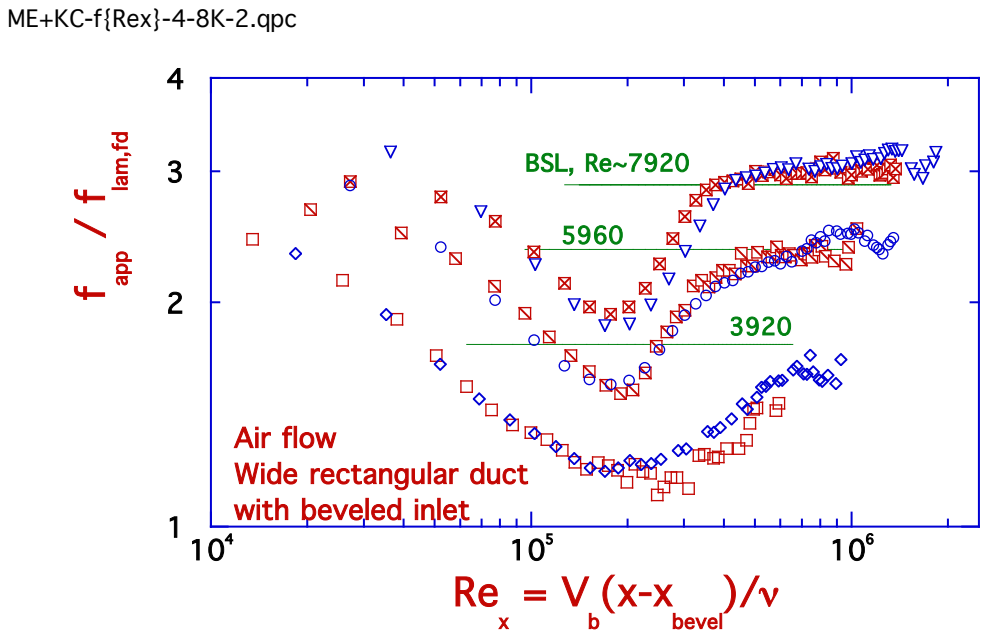

Fig. 10. Some present measurements of development of local apparent friction factors presented as functions of the streamwise Reynolds number with logarithmic coordinates. See text for explanation of symbols.

One sees that in the entry region ahead of the transition onset the slopes are approximately the same and are comparable to those of the pre-transition laminar results of Nolan and Zaki (even though the data are for $f_{app}\{x\}$ while the DNS of Nolan and Zaki present $C_f\{x\}$ defined in terms of τ_W). For the two-dimensional numerical predictions of Schade and McEligot the near-asymptote at small x (calculated from the first two points) gives a slope $m \approx -0.36$ for the duct friction factor based on wall shear stress $f_S\{x\}$, less steep than the Blasius laminar solution, $C_{f,x} \approx 0.664\ Re_x^{-1/2}$ (e.g., eqn. 4-52 by White [text 1991]). One difference between the laminar entry region and a Blasius boundary layer is that the duct entry flow has a streamwise pressure gradient whereas the Blasius solution assumes zero pressure gradient; therefore exact agreement is not expected. However, it is interesting that, for the near-asymptote of $f_{app}\{x\}$, $m \approx -0.48$ is predicted by Schade and McEligot, close to the Blasius solution. The following slopes are estimated manually from pertinent figures. For their range $0.002 \le (4x/(D_h Re Pr)) \le 0.01$ (approaching transition onset) the slopes are predicted to be $m \approx -0.45$ for $f_{app}\{x\}$ and $m \approx -0.38$ for $f_S\{x\}$. The three-dimensional time-dependent DNS for bypass

transition by Nolan and Zaki [JFM 2013] show approximate slopes of $C_f\{Re_x\}$ approaching transition onset as $m \approx - 0.38$ for their case with zero streamwise pressure gradient and $m \approx - 0.4$ for the favorable pressure gradient in Figure 9. As shown by Klebanoff, Tidstrom and Sargent [JFM 1962], Blackwelder [Phys.Fl. 1983], Herndon, Walsh and McEligot, IJHFF 2007, Walsh et al. [JFE 2011], Zaki and colleagues and others, some differences between the Blasius conditions and transitioning laminar boundary layers with zero pressure gradients are that the latter have streamwise vortices and turbulent fluctuations that modify the mean velocity profile and other statistics; these phenomena are expected in the present entry flow also. As an example of the present data, in Figure 10 the estimated slope of $f_{app}\{x\}$ for the four mm run at $Re_{Dh} \approx 5960$ is $m \approx - 0.38$ again approaching transition onset.

Beyond transition onset the two pairs of turbulent runs show approximately the same increasing slopes ($m \approx 0.69 \approx 0.7$ or maybe 2/3) in the initial part of the transition growth curve. The lower Reynolds number runs have lower slopes representing more gradual growth. Several popular correlations for the length of the transition growth curve (aka "transition length") are phrased in terms of the momentum thickness or other quantities which cannot be calculated from the present measurements [Mayle, J.Turbo. 1991; Qui and Simon, ASME paper 97-GT-455]. So in the present work the transition length is examined in terms of the local Reynolds number based on streamwise distance in Figure 10. For the three pairs of data the non-dimensional distance to developed onset generally decreases as Re_{Dh} increases. Since $Re_{x,tr}$ is approximately constant there, their transition lengths also decrease with Re_{Dh}.

The data of Figure 10 are presented with a linear abscissa in Figure 11 to emphasize the downstream behavior. Since the test section length is fixed physically, the non-dimensional length V_bL/ν increases as V_b increases from higher Re_{Dh} and smaller spacing (three vs. four mm). One sees the four upper runs reach approximately constant levels of $f_{app}\{x\}$, representing fully-developed local streamwise pressure gradients (i.e., apparent wall shear stresses). It is not clear whether the three mm case at $Re_{Dh} \approx 3950$ attains this condition or not; if it does, it disagrees with the turbulent correlation of Beavers, Sparrow and Lloyd by about eight per cent (not shown). The four mm run at $Re_{Dh} \approx 3920$ does not complete transition before the end of

the test section, In this figure, to the eye, it appears that for the turbulent pairs of runs the four mm cases reach developed onset at a smaller value of Re_x than their companion three mm ones; since the location of developed onset is a measure of the hydraulic entry length, the generality of this observation will be examined later with estimates for more flow rates.

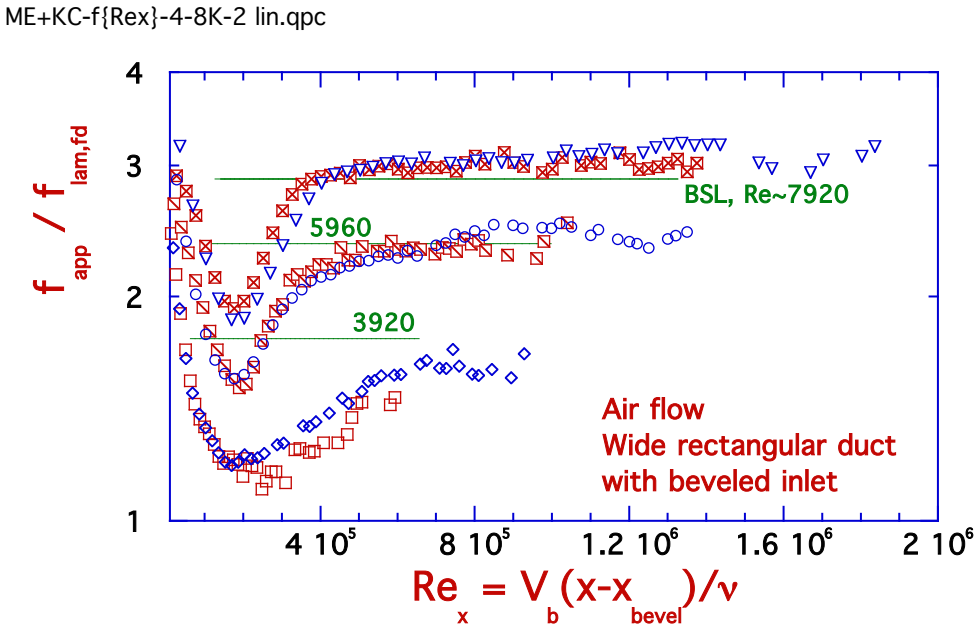

Fig. 11. Data of Figure 10 expressed with a linear abscissa to emphasize the downstream region.

Presentation simply as $f_{app}\{Re_X\}$ collapses the data somewhat towards a single function, particularly for the turbulent cases, as shown in Figure 12. This figure includes the same data as Figure 10 with the same symbols except the four mm case from the transition region is omitted for clarity. As in Figure 10 transition onset is typically slightly below 2 $x10^5$ for these cases.

Since the downstream turbulent results agree approximately with the BSL correlation, $f_{fd,BSL} \approx 0.1268 / Re_{Dh}^{0.3}$, the trend there is for f_{fd} to decrease as Re_{Dh} is increased. For the range of Re_{Dh} included. the BSL correlation varies by about twenty per cent. In this presentation, the data in the laminar entry region upstream of transition onset shows the same trend as the developed turbulent region, i.e., $f_{app}\{Re_X\}$ decreases as Re_{Dh} increases by roughly the same amount (except near transition onset).

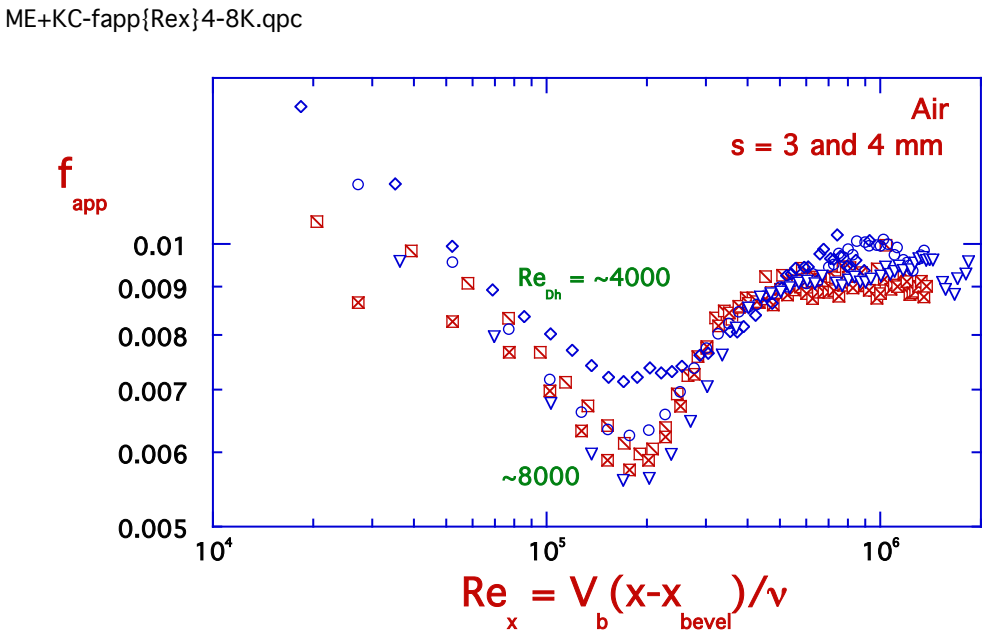

Fig. 12. Development of local apparent friction factors without normalization of the ordinate. Same cases as Figure 10 with same symbols.

Figure 13 examines the results of Figure 12 when normalized by the downstream turbulent correlation of Beavers, Sparrow and Lloyd. If the downstream data agreed exactly with the correlation, the turbulent runs would converge to unity at large streamwise Reynolds numbers; however, the cases at our higher Re_{Dh} tended to have slightly higher $f_{app,fd}$ measurements than the correlation as mentioned earlier and as shown in Figure 3 for the downstream series. For the four turbulent runs, the behavior in the pre-transition "laminar" region and at transition onset seem to collapse better than $f_{app}\{Re_X\}$ without normalization in Figure 12. In general, this normalization shows some trends opposite to those for $f_{app}\{Re_X\}$ not normalized; for example, in addition to downstream, the entry region values increase slightly with Re_{Dh} rather than decreasing. For engineering estimates of the turbulent cases, it appears from a linear plot (not shown) that one could choose a single curve to represent the entry region to the developed onset; whether this observation has more generality than the present limited ranges would require more experiments or DNS.

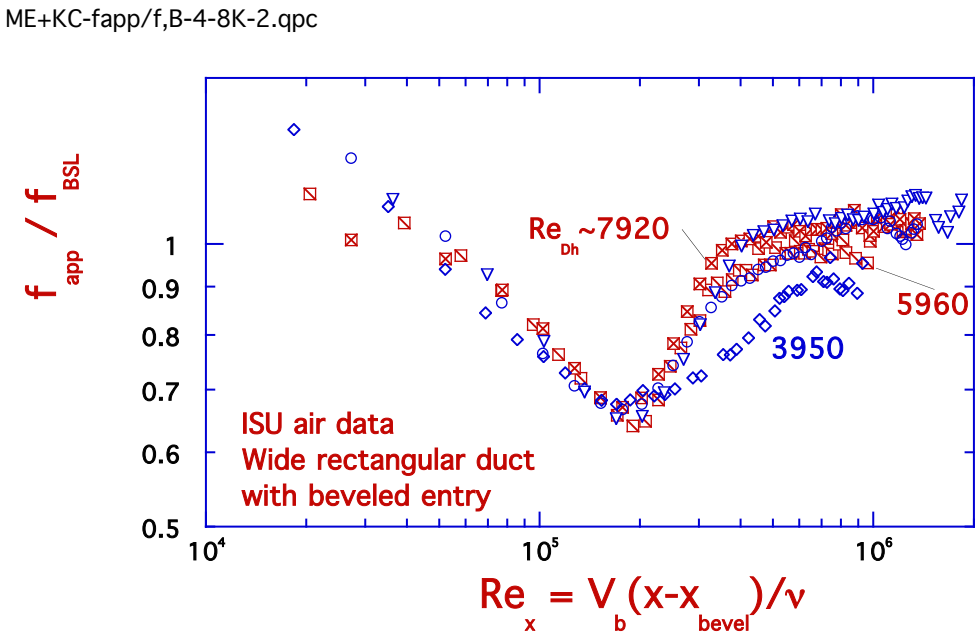

Fig. 13. Streamwise development of local apparent friction factors normalized by the downstream turbulent correlation of Beavers, Sparrow and Lloyd [J.Basic.Eng. 1971] for the same five cases as Figure 12 with the same symbols.

5.4. Locations of transition onset

Several *observations from the preceding streamwise figures are summarized* in terms of laminar coordinates and streamwise Reynolds numbers in Figures 14a and b, respectively. In each figure the abscissa is the Reynolds number based on hydraulic diameter, a non-dimensional mass flow rate. The data for transition onset are provided by circles for the three mm test section and by squares for the four mm one. For developed onset (or the beginning of apparently fully-developed turbulent flow) the three mm estimates are shown by diamonds and four mm by crossed squares. For the idealized laminar duct entry behavior predicted by Schade and McEligot [IJHMT 1971] an entry length can be taken as the distance where f_{app} has decreased to within two per cent of the fully developed value, $((x - x_{bevel})/(s\ Re_{Dh})) \approx 0.035$ approximately, as shown by short dashes on Figure 14a. Converted to a streamwise Reynolds number in Figure 14b, this location is denoted by the shortest dashes for the four mm test section and by the next shortest dashes for the three mm one. While that entry length is not necessarily the same as

some defined boundary layer thickness at the centerplane, it can be expected to show the same trends. The other dashed lines --- which show the downstream ends of the test sections in the appropriate non-dimensionalization of the particular subfigure --- are labeled accordingly.

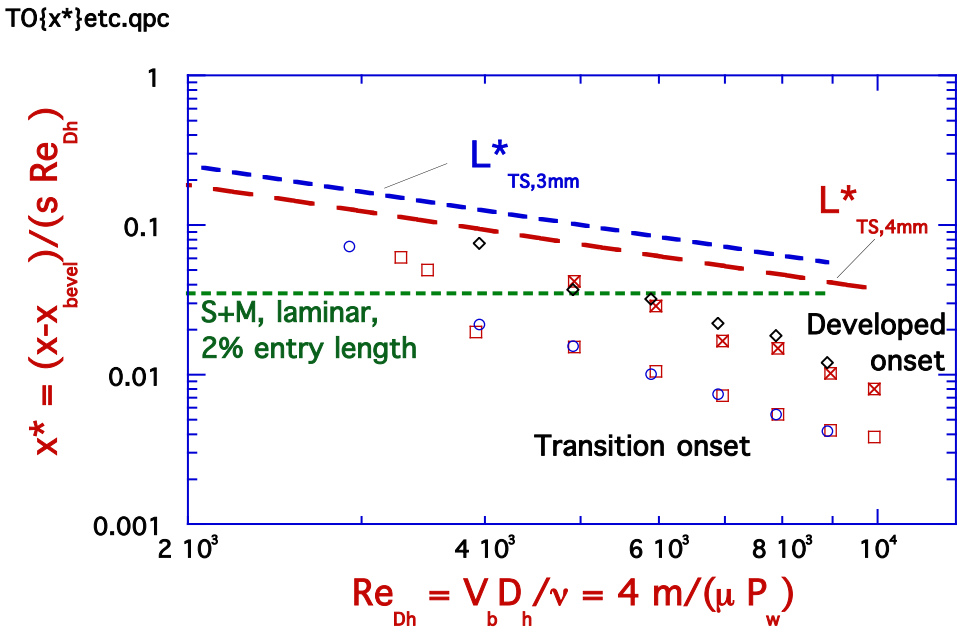

Fig. 14a. Some characteristics of transition in a wide rectangular duct with a converging entry measured in terms of streamwise laminar coordinates. See text for explanations of symbols.

For $Re_{Dh} > \sim 4000$, upstream of the 2% entry length Fig 14b shows that transition onset occurs at about the same value of Re_x so transition is believed to begin where the near-wall flow behaves as a boundary layer rather than a developed flow. Thus, in laminar coordinates (Figure 14a) the location x_{to}^* decreases approximately as Re_{Dh}^{-2} since the two coordinate systems are related as $x^* = (2/ Re_{Dh}^2) Re_x$, For these spacings, below $Re_{Dh} \approx 4000$ the few runs which experience transition before the end of the test section show transition onset downstream of the 2% laminar entry length, i.e., in the nearly-developed laminar flow; $Re_{x,to}$ is about eighty per cent further downstream than the boundary layer cases at higher flow rates. At lower Re_{Dh} than the data shown here transition is not apparent before the end of the test section, if ever.

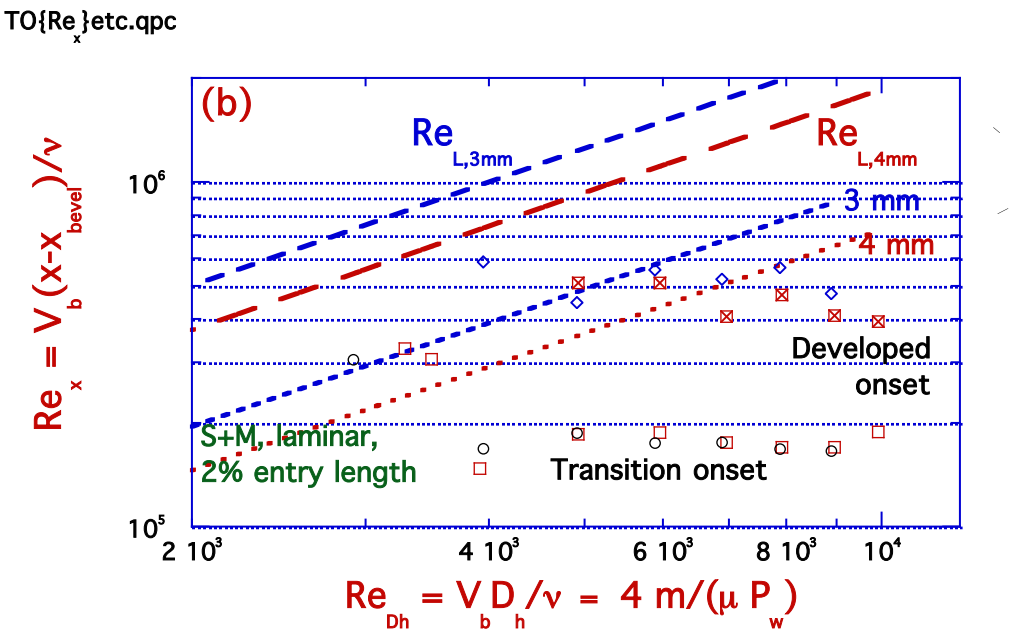

Fig. 14b. Some characteristics of transition in a wide rectangular duct with a converging entry measured in terms of streamwise Reynolds numbers. See text for explanations of symbols.

Estimates of developed onset are roughly constant values in terms of Re_X, although more scattered than transition onset due to the difficulty in determining these values from the scattering of the experimental results; one can approximate these results as $Re_{X,do} \approx 5 \times 10^5$ (+/- 20 %). Consequently, the locations of developed onset also appear to vary as Re_{Dh}^{-2} in terms of laminar coordinates x* (Figure 14a).

We could also consider developed onset to represent an entry length for the streamwise pressure gradient of flows that undergo transition in the duct. From these figures we see that -- for the present higher Re_{Dh} data --- its fully-developed turbulent flow occurs upstream of where a laminar flow at the same Re_{Dh} would become (nearly) fully-developed. At somewhat lower Re_{Dh} these entry lengths would be about the same for laminar and transitional/turbulent flows and for $Re_{Dh} \approx 4000$ the streamwise pressure gradient of a laminar flow would become developed upstream of a transitional/turbulent one. For $Re_{Dh} \approx 3500$ and less, transitional flow

reaches the end of the test section before achieving the fully-developed turbulent condition defined here (i.e., constant $f_{app}\{x\}$).

6. Concluding remarks and discussion

In order to address a primary ***aim*** of obtaining insight into the apparent evolution of flow regimes at moderate Reynolds numbers in thin, wide rectangular ducts with converging inlets, fundamental streamwise pressure distributions were measured. The convergences were formed by planar bevels on the opposed wide surfaces and the working fluid was air at laboratory temperatures. Ducts of 3.030 and 4.077 mm spacings s, giving non-dimensional lengths of (L/s) ≈ 500.8 and 372.2 and widths (W/s) ≈ 114.6 and 85.19, respectively, were compared. Flow rates ranged from Re_{Dh} of about 980 to 10,020 and corresponding non-dimensional downstream pressure gradient parameters ($-K_p$) covered the range 0.038 to 0.0061, respectively. Primary measurements are the streamwise pressure distribution P{x}, the air temperature and the mass flow rate.

In an attempt to obtain data for *fully-developed friction factors*, the pressure drop between two downstream pressure taps was used to calculate an $f_{app,ds}\{Re_{Dh}\}$ as many investigators have done in the past. The two taps were at $((x-x_{bevel})/s) \approx 206.7$ and 470 for the three mm spacing and 154 and 351.5 for four mm. At low Re_{Dh}, results from both test sections agreed with the laminar fully-developed predictions and for the high Re_{Dh} they showed approximate agreement with the correlation of Beavers, Sparrow and Lloyd [J.Basic.Eng 1971] for fully-developed turbulent flow in comparable ducts. In the region taken as turbulent, the slope of the present data appears to be slightly greater than the BSL correlation, corresponding to the DNS predictions of Kawamura and colleagues [Tsukahara et al., WCCM VI 2004, 1IFHT 2004] (e.g., see Figure 4 of McEligot and Johnson [NERS 2017]). In the intermediate range of Re_{Dh} apparently the transition process started before the downstream pressure tap but had not been completed before the first one so a fully-developed state may not have been established for the whole measured length. Also, in this intermediate region the values of $f_{app,ds}\{Re_{Dh}\}/f_{fd,lam}\{Re_{Dh}\}$ for the three mm case are slightly, but discernably, higher then those of the four

mm case. For three mm, apparently transition starts *within the test section length* for Re_{Dh} greater than about 2700 and $f_{app,ds}\{Re_{Dh}\}$ appears to correspond to the fully-developed turbulent region *before the first pressure tap* for Re_{Dh} greater than about 5600. The corresponding values for the four mm case are $Re_{Dh} \approx 3000$ and 5900. *If the location of the first pressure tap were changed, the values of Re_{Dh} determined for the onset of fully-developed turbulent flow would change accordingly*. The downstream pressure gradient parameter data indicated that the flow would remain laminar if $(-K_{p,ds})$ is 0.022 or greater for the three mm test section or 0.021 or greater for the four mm case; these values are about the same magnitude as Bankston [JHT 1970] suggested for heated turbulent gas flow in circular tubes.

The *hydraulic entry behavior* of the constant cross-section duct downstream of the edge of the inlet bevel *showed apparently laminar flow initially for all experiments* in the detailed series where local $f_{app}\{x^*\}$ could be calculated. These entry data followed (above) the numerical predictions of Schade and McEligot [IJHMT 1971] for laminar flow in the entry of an infinitely-wide parallel plate duct with a uniform entry velocity. For $Re_{Dh} \approx 3300$ or greater the measurements have minima in local $f_{app}\{x^*\}$ that we define as "transition onset;" these runs, which apparently undergo transition towards turbulent flow, typically have values of $f_{app}\{x^*\}$ about ten to twenty per cent higher than the results of S+M in their laminar entry.

Examining the data with the streamwise Reynolds number as the ordinate demonstrates that, for $Re_{Dh} \approx 4000$ or greater, transition onset is near constant around $Re_{x,to} \approx 1.7 \times 10^5$. As a consequence, in laminar coordinates $x_{to}^*\{Re_{Dh}\}$ systematically increases as Re_{Dh} decreases since the two coordinate systems are related as $x^* = 2\ Re_x / Re_{Dh}^2$, For lower Re_{Dh}, where the present measurements would be near the 2% entry length of S+M before apparent transition, $Re_{x,to}$ is about eighty per cent further downstream. We suspect that the higher Re_{Dh} results correspond to transition being initiated in a near-wall boundary layer growing in the hydraulic entry. Estimates of the location of developed onset (or the beginning of apparently fully-developed turbulent flow) are also roughly constant values in terms of Re_x, although more

scattered than transition onset; one can approximate these results as $Re_{x,do} \approx 5 \times 10^5$ (+/- 20 %).

As a by-product of the experiment, a *secondary objective* --- to assess design-style CFD predictions from a popular "standard k-ε two-layer turbulence model" --- could also be pursued. As such, the CFD predictions of Johnson [ASME paper IMECE2011-65831; McEligot and Johnson, NERS 2017, say M+J] for a comparable geometry are assessed. For flows assumed to be laminar, the turbulence model was suppressed beginning at the streamwise end of the inlet bevel. For turbulent flow the code employed the "standard k-ε two layer turbulence model with the all y^+ wall treatment" throughout. The flow was assumed to be fully-turbulent for Re_{Dh} = 2600 and higher based on the transition data of Patel and Head [p 186, JFM 1969]. For both laminar and turbulent entry flows the apparent friction factors predicted by the code started above the downstream fully-developed values and decreased monotonically to their constant values of $f_{app,fd}$ downstream (their Figures 3 and 5). Their *laminar* CFD entry results for a six mm duct agreed approximately with the numerical entry predictions of Schade and McEligot [IJHMT 1971], say S+M. Figure 3 by M+J presents these CFD predictions; they show the same trends in the immediate entry as the present four mm data in our Figure 5 but converge with the numerical predictions of Schade and McEligot at a lower value of x* than the measurements.

The *turbulent* k-ε CFD predictions for $Re_{Dh} \approx 3040$ with six mm spacing over-predicted the present friction factor data for $2910 < Re_{Dh} < 3090$ by about a factor of two as seen in Figure 5. This difference is mainly because the CFD calculations assumed the flow to be fully-turbulent whereas the experiments showed the flow to appear to be laminar or barely transitional in this range. The other k-ε prediction by Johnson is compared to present data at the upper end of our "transition range" in Figure 7. His ten mm duct flow at $Re_{Dh} \approx 5320$ is compared to pairs of data at $Re_{Dh} \approx 4900$ and 5900, a grouping that brackets its non-dimensional flow rate (Re_{Dh}). The CFD results again over-predict the entry $f_{app}\{x\}$ because it is treated as a turbulent flow with a growing turbulent boundary layer rather than the laminar entry flow implied by the experiments. As shown by Figure 4 of M+J, the fully-developed results of this k-ε model are predicted to exceed the DNS values of Kawamura and colleagues by ten per cent *or more* for

Re_{Dh} less than about 5600. While the laminar CFD predictions gave reasonable results as might be expected, in general the k-ε model over-predicted $f_{app}\{x^*\}$ upstream of developed onset for the transitional and turbulent flows measured. The k-ε calculations predict a turbulent entry length of about forty spacings but the experiments indicate it can be much longer.

For improved CFD predictions in the present Re_{Dh} range, the transition process must be treated adequately. Abraham and colleagues [IJHMT, 2009, 2011; JFE 2019; Minkowycz, Abraham and Sparrow, IJHMT, 2009] have included a transition model in their CFD code to predict laminar, transitional and turbulent flows successfully for a variety of geometries. It would be desirable to assess Abraham's technique and/or comparable ones for the geometry of the present experiments (as attempted by Rehman, Morini and Hong [Micromach. 2019] for a microchannel experiment) but that extension is beyond our scope. Assessing recent large eddy simulation (LES) approaches, as by Choi et al. [Phys.Fl. 2022], would also be desirable.

With a test section consisting of plates about 350 mm (1.1 ft) wide spaced three mm (~1/8 inch) apart and a limited budget, it was not practical to measure pointwise velocities in the present experiments. However, it appears that --- for $Re_{Dh} > \sim 4000$ --- transition would have occurred in the growing near-wall boundary layer. So while the present experiment does not provide pointwise velocity distributions, we can obtain insight into the developing flow phenomena in the entry region at the higher Re_{Dh} by considering the transition as "bypass transition," i.e., transition primarily induced by strong freestream turbulence [Morkovin 1969; Klebanoff, Bull.APS 1971; Walsh et al., JFE 2011; Zaki, FTC 2013] (assuming an entry separation bubble has induced turbulence in its shear layer) and employing available DNS of representative bypass transitional boundary layers such as those of Zaki and colleagues [FTC 2013; Nolan and Zaki, JFM 2013; Hack and Zaki, JFM 2016]. Their results have moderate inlet freestream turbulence of about three per cent and several streamwise pressure gradients; inlet conditions include a Blasius velocity profile at $Re_{x,0} \approx 26{,}600$ for all cases discussed by them. Examination of their predicted wall friction distributions shows comparable trends to the present experiments that we surmise to be possible indications of the presence of the same

phenomena / structures. In general we will be discussing qualitative comparisons rather than quantitative ones since turbulence levels were not measured in the present experiments.

Figure 15 presents the Nolan and Zaki DNS predictions of the streamwise evolution of the skin friction coefficient C_f for a flow with zero pressure gradient and one with a favorable pressure gradient, both compared to laminar predictions from application of a Thwaites/Falkner-Skan (T/FS) technique [Philos.Mag. 1931; Aero. Qtly. 1949; Schlichting 6, 1968; White 2, 1991]. The T/F-S approach is effectively a two-dimensional calculation where the wall-normal transport of streamwise momentum is only by molecular shear. In contrast, the direct numerical simulations are three-dimensional and temporal providing instantaneous spanwise velocities as well so they can account for momentum transport by advection, such as streamwise vortices, and turbulent fluctuations also. One can see that the DNS cases diverge above the T/F-S predictions between the inlet boundary and transition onset; nearing transition onset the difference grows to about ten to fifteen per cent. This growing difference corresponds to the appearance and growth of "high- and low-speed streaks" in the boundary layer. For example, in Figure 19 by Nolan and Zaki [JFM 2013] streaks with close spacing appear within a few boundary layer thicknesses of the inlet and then their spacing grows irregularly in the streamwise direction; the spacing between adjacent streaks can be taken as an indication of the sizes of the streamwise vortices that form the streaks. With their "Simple Pseudo-Vortical Motion model," Kasagi, Hirata and Nishino [Exp.Fl. 1986; McEligot et al., IJHMT 2020] have demonstrated that streamwise vortices show good agreement with the vorticity field in viscous wall regions. Thus, another hypothesis for the present differences between the two-dimensional S+M prediction (which cannot include 3-D streamwise vortices) and the measured values of $f_{app}\{x^*\}$ upstream of transition onset could be that the flow and resulting mean velocity field there is dominated by a system of streamwise vortices which yield lower resistance to transport of streamwise momentum in the wall-normal direction (e.g., Figure 12b by McEligot et al. [IJHMT 2020]) and, hence, higher wall friction.

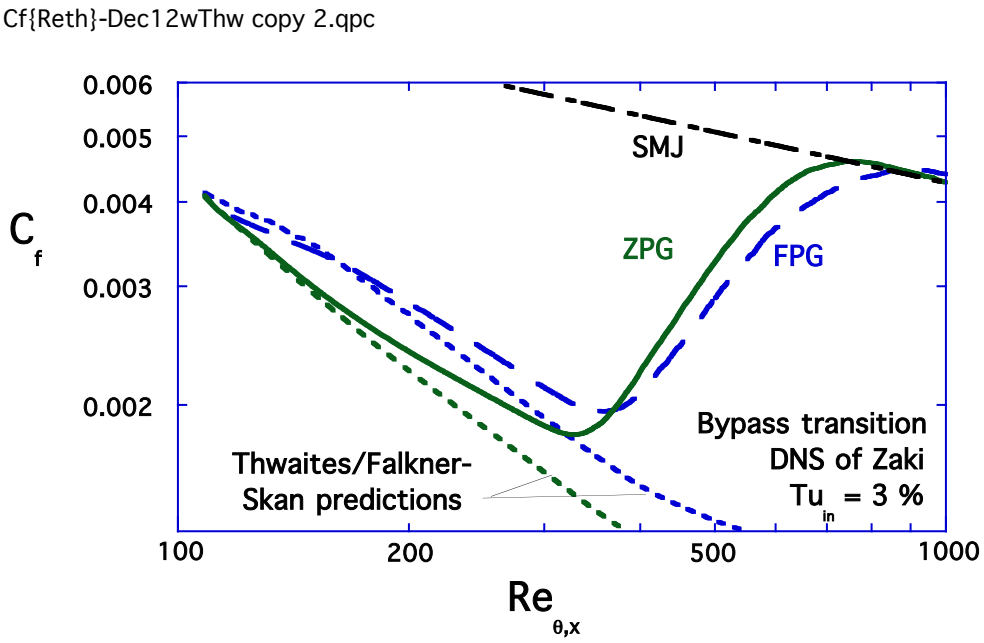

Fig. 15. Comparison of three-dimensional DNS results of Nolan and Zaki [JFM 2013] for bypass transition to two-dimensional theoretical predictions by the "Twaites/Falkner-Skan approach," e.g., see White [text 1991], (short dashes). Centerline markings labeled "SMJ" are the turbulent correlation by Smits, Matheson and Joubert [J.ShipRes. 1983].

The plenum upstream of the beveled inlet is about 350 mm across in the y-direction and the intersection of the plenum wall with the beveled inlet has an included angle of about 115.9 degrees. To the flow from the plenum the intersection of these two surfaces appears like a perpendicular two-dimensional ridge which may induce curvature of the mean streamlines around it. The same situation occurs at the bevel's downstream edge intersecting with the surface of the rectangular duct. Scorer's analysis [IMA J.Appl.Math. 1967] of local instability in curved flow "shows that . . . in general curved flow in two dimensions . . . most likely disturbances are . . . longitudinal rolls." However, it is believed that the flow in the upstream plenum is turbulent with the acceleration in the converging inlet acting to laminarize it. A resulting question is --- whether streamwise vortices form as part of the laminarizing process, whether the flow becomes essentially laminar before vortices are formed or whether vortices are not formed until well along in the rectangular duct. That is, where do the streamwise vortices, that apparently are precursors to the transition in the duct, first form in this geometry?

The mean distribution of the skin friction evolution predicted by the DNS for the ZPG case by Nolan and Zaki [JFM 2013], say N+Z, is shown in Figure 16a in comparison to the classic two-dimensional prediction of Blasius. (Also shown for later comparison are some present data in Figure 16b.) The inlet condition of the DNS is an imposed Blasius mean velocity profile so the two curves match at $Re_{x,in} \approx 2.66 \times 10^4$. The three-dimensional DNS results then diverge "upwards" very gradually until near $Re_x \approx 6.2 \times 10^4$ where it begins a straight line behavior (in the logarithmic coordinates) which persists until about $Re_x \approx 1.7 \times 10^5$ approaching our defined transition onset. This straight line section can be described as "power law behavior" which can be considered to imply an effect of an organized structure of some sort in the developing flow. In discussing their Figure 7 of conditionally-sampled C_f, N+Z attribute the difference to "mean flow distortion by Klebanoff streaks." After the transition onset (= $C_{f,min}$ at $Re_{x,to} \approx 2.02 \times 10^5$) another straight line evolution can be discerned over the approximate range $\sim 2.6 \times 10^5 < Re_x < \sim 3.7 \times 10^5$.

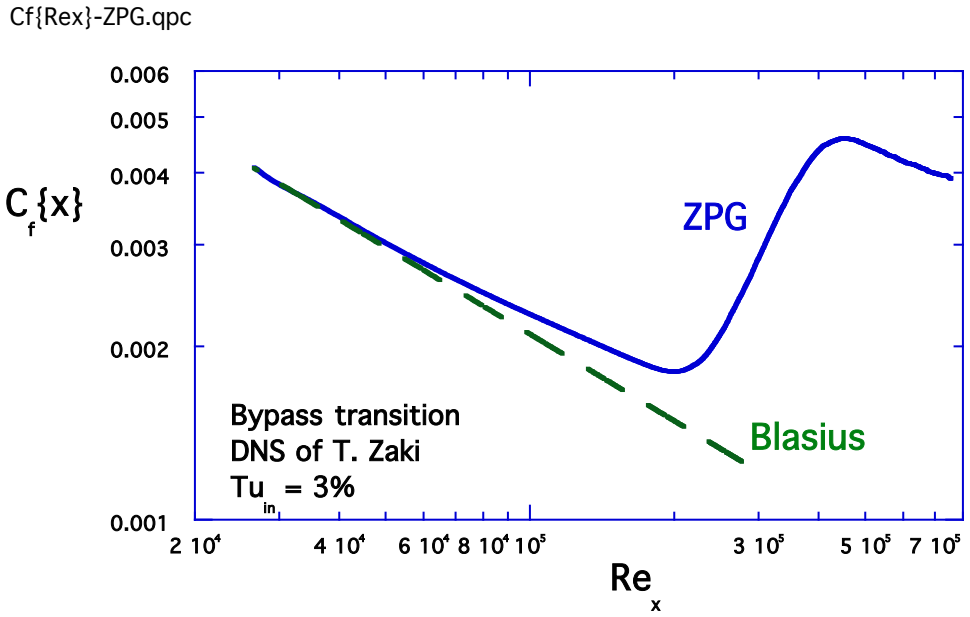

Fig. 16a. Comparison of skin friction evolution for negligible streamwise pressure gradient predicted by three-dimensional DNS of Nolan and Zaki [JFM 2013] to classical two-dimensional solution by Blasius.

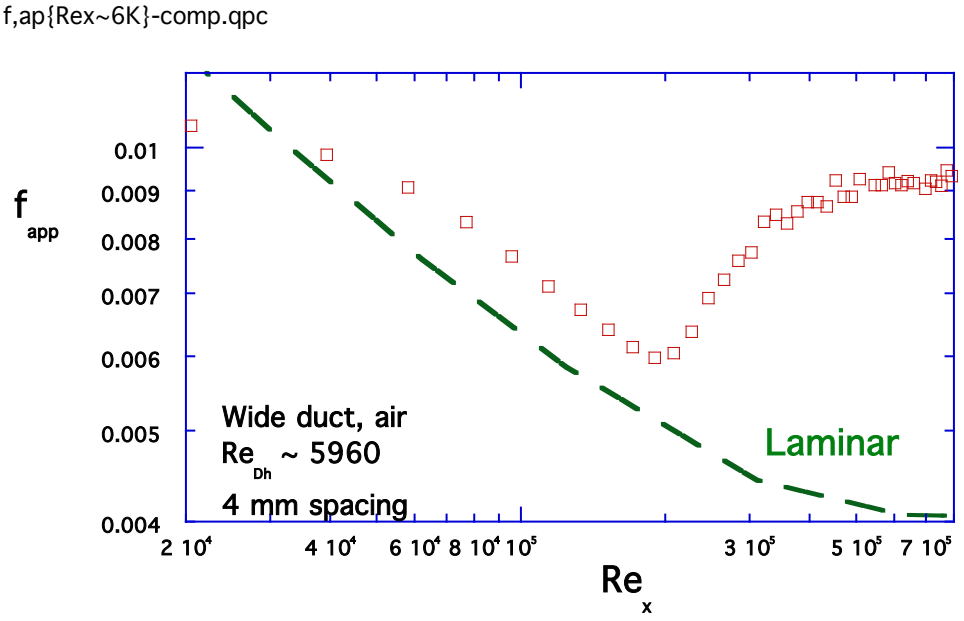

Fig. 16b. Example of comparison of apparent friction factor evolution for present experiment to two-dimensional numerical prediction of laminar hydraulic entry by Schade and McEligot [IJHMT 1971].

Instantaneous Figure 19 (bottom) of N+Z shows a few negative streaks starting at their $(x\text{-}x_0) \approx 10$ ($Re_X < \sim 3.5 \times 10^4$) then mostly alternating with positive streaks and evident until their laminar-turbulent edge at $(x\text{-}x_0) \approx 400$ or $Re_X \approx 3.5 \times 10^5$ (N+Z define their non-dimensional x as x/δ_{in}). We interpret alternating negative and positive "Klebanoff streaks" as identifying streamwise vortices as do Bakewell and Lumley [Phys.Fl. 1967], Blackwelder and Eckelmann [JFM 1979] and others. So this location of likely streamwise vortices corresponds to the pre-transitional straight-line section of $C_f\{Re_X\}$.

In their study of entropy generation in bypass transition with streamwise pressure gradients from the DNS of Nolan and Zaki [JFM 2013], McEligot et al. [in preparation 2024] observe that, "as far as entropy generation is concerned, the main effects of the transition process are (1) to shrink the physical size of the viscous layer which provides most of the entropy generation in the form of direct (mean) dissipation and (2) to initiate a turbulent layer which

provides additional entropy generation, mostly as indirect (turbulent) dissipation" as the outer region of the boundary layer.

While we define the "transition onset" as a minimum in C,f{Re} for convenience, the curvature of C,f{Re} on a logarithmic graph of the data is evident further upstream, indicating a potential change in the near-wall flow structure. Thus, it can be argued that our transition onset is not actually the onset of transition (depending on the phenomenon being used as an indication in the definition). An alternate definition could be that transition onset is at the location where turbulence (other than freestream turbulence) is first observed by the measurement technique used (e.g., consider Nolan, Hack and Marxen observations).

For the ZPG case in their Figure 27 (middle) N+Z show turbulent spot inception possibly as early as $(x\text{-}x_0) \approx 160$ or $Re_x \approx 1.5 \times 10^5$ and their intermittency observably greater than zero at $(x\text{-}x_0) \approx 190$ or $Re_x \approx 1.8 \times 10^5$. One could interpret this information as indicating that the initiation of curvature (or increase in slope) of $C_f\{Re_x\}$ ahead of the defined transition onset is caused by the first turbulent spots appearing (say onset of turbulent spots?). Their Figures 5 (ZPG), 27 (top ZPG) and intermittency (middle of Figure 27) indicate that their ZPG boundary layer is completely turbulent by $(x\text{-}x_0) \approx 550$ or $Re_x \approx 4.7 \times 10^5$. Their intermittency distribution $\gamma\{x\}$ has a straight line section over the range $\sim 2.3 \times 10^5 < Re_x < \sim 3.9 \times 10^5$ corresponding to the straight line region of $C_f\{Re_x\}$ downstream of transition onset.

Also of interest in the N+Z results are the instantaneous skin friction values in the vicinity of turbulent spots shown in their Figure 8 (bottom left). For the turbulent spot of interest, a high value of the laminar-conditioned C_f appears within the upstream edge of the spot. For the turbulent region starting at their $(x\text{-}x_0) \approx 400$, high values of the laminar-conditioned C_f occur upstream of the turbulent-laminar interface of the "spot" as well as within its upstream section. This behavior is possibly due to some convergence of laminar flow near the spots, transition of large streamwise vortices into smaller ones or some other explanation. Marxen and Zaki [JFM 2019] have examined the structure and turbulent statistics of isolated spots in the early stages of transition in ZPG cases by conditional and ensemble averaging. At low

maximum intermittency factors upstream ($\gamma_{max} \approx 0.1, 0.25, 0.5$) in their Figure 14, the turbulent-conditioned u_{rms}^{+} profiles are higher than for fully-developed turbulent boundary layers, being highest at the upstream location, possibly due to "influence of the pre-transitional high-amplitude Klebanoff distortions" according to M+Z. Further analysis of the spatial and temporal vicinity of the upstream region of early turbulent spots could be desirable to resolve these possibilities but is beyond the present scope.

The estimates in the above several paragraphs have been taken from some very small graphs so the numerical values should be taken with several grains of salt.

For the most part, the present data for flow in the hydraulic entry of a wide rectangular duct show the same features as the DNS of bypass transition by N+Z as shown in our Figure 16b for $Re_{Dh} \approx 5960$. The appropriate laminar comparison is to a two-dimensional numerical hydraulic entry prediction for a duct as by S+M (shown) and others. (The conversion from the entry coordinates of S+M to Re_x is given by $Re_x = (Re_{Dh}^2 / 2)\, x^*$.) There are two obvious differences. First, in the turbulent downstream region the present data attain a constant level of $f_{app}\{x\}$ as it reaches a fully-developed condition in the confined duct of constant cross section while the DNS is for an "unconfined" boundary layer which keeps growing. Second, in the pre-transitional laminar region the straight-line behavior of the data is approximately parallel to the two-dimensional laminar prediction rather than diverging gradually as the DNS results do. Earlier we mentioned that, in the present geometry, a laminar wall boundary layer apparently begins developing after the suspected separation bubble downstream of the edge of the inlet bevel (or at the bevel edge or along the bevel if there is no separation bubble) if transition has not already been initiated in the free shear layer between the bubble and the core flow. In addition to these possibilities and different mean velocity profiles at the inlet, it is feasible that streamwise vortices already exist at $x^* = 0$ in the experiment due to flow curvature around the corner there, e.g., see Scorer [IMA J. Appl. Math. 1967].

Hack and Zaki [JFM 2016] found approximate similarity of some variables in terms of the momentum thickness for three pressure gradients: their FPG, ZPG and APG-2. Plotting as

functions of (θ/θ_0) collapsed DNS results for streak attributes such as peak amplitudes, spanwise and wall-normal shear and their defined sweep cross-sectional areas (their Figure 9). In particular, they found the position of their transition onset (= $C_{f,min}$) to be about $(\theta/\theta_0) \approx 3$ for each of the three flows while $Re_\theta\{C_{f,min}\}$ differs noticeably for them thanks to their differences in U_∞ (their Figure 3b). Figure 17 reveals a few more approximate similarities in terms of the skin friction behaviors as functions of the momentum thickness. One can identify straight-line sections approaching transition onset in the pre-transitional laminar region; the initiation of curvature at the ends of these lines or likely onset of turbulent spots occurs at approximately the same value of (θ/δ_{in}) for the three cases. Downstream the $C_f\{\theta\}$ values in the asymptotic turbulent region collapse for the three pressure gradients (as might be expected since the values of their non-dimensional pressure gradients K_p are all "small" in this region as shown in Figure 18). And the onset of this asymptotic turbulent behavior is near the same momentum thickness for the three pressure gradients (within about ten per cent). One wonders whether the momentum thickness would also serve as an approximate similarity variable somehow for the present data but, again, our experiment does not provide the mean velocity distributions needed to check.

To assess the foregoing speculations, further direct numerical simulations are recommended, addressing the present geometry including plenum and inlet and utilizing adequate spanwise resolution. Alternatively, it may be possible to model the configuration in an experiment using a different fluid as by Eckelmann who employed Reichart's apparatus decades ago [JFM 1974] but it probably would be gigantic.

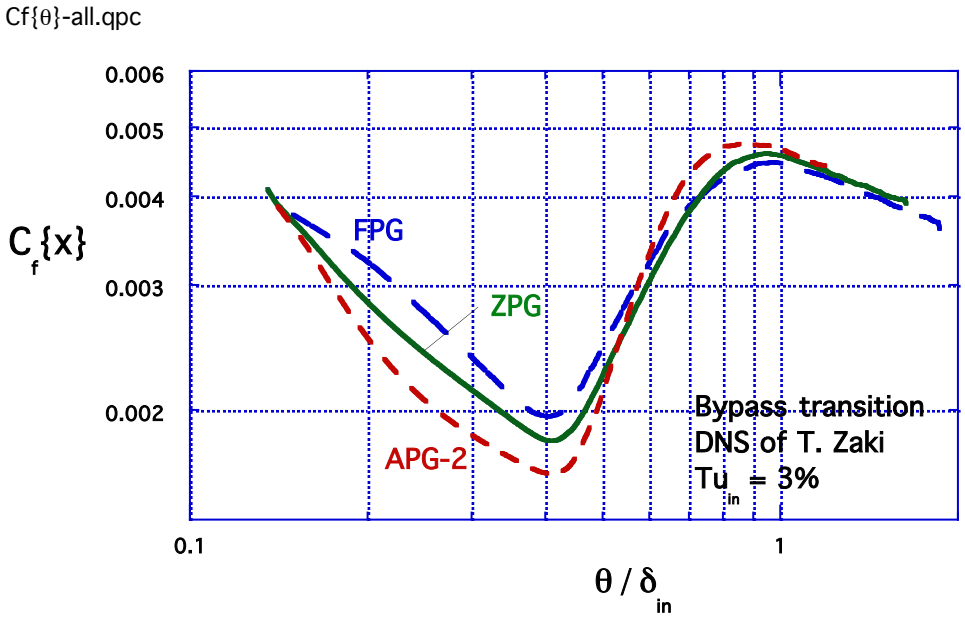

Fig. 17. Effect of streamwise pressure gradient on skin friction evolution predicted by DNS of Nolan and Zaki [JFM 2013] when presented in terms of momentum thickness as a possible similarity parameter suggested by Hack and Zaki [JFM 2016].

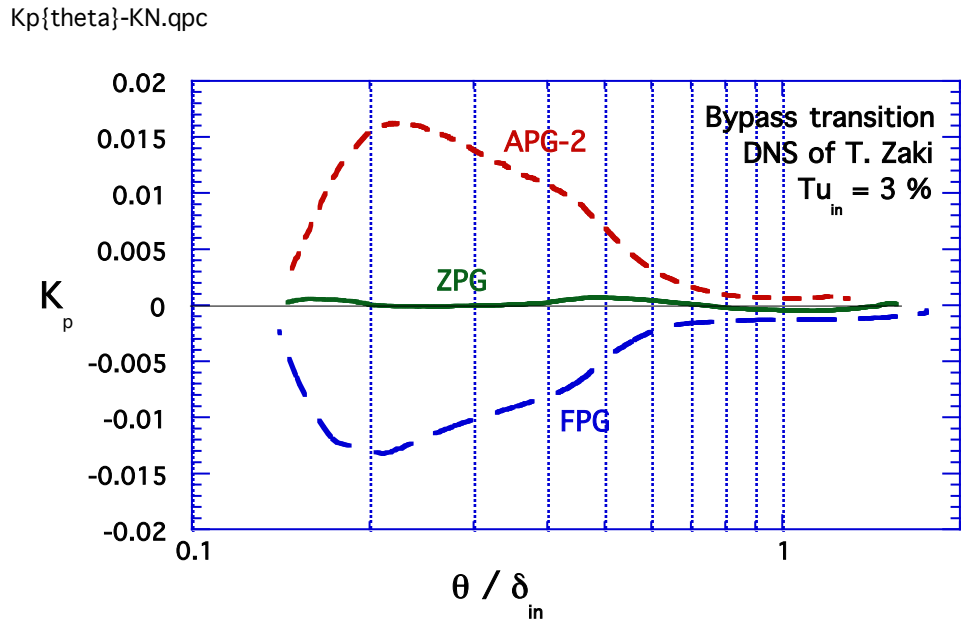

Fig. 18. Streamwise variation of non-dimensional pressure gradient for the three cases predicted by the DNS of Nolan and Zaki [JFM 2013] when presented in terms of momentum thickness as a possible similarity parameter suggested by Hack and Zaki [JFM 2016].

Acknowledgements

In addition to the present authors, substantial assistance on the experiments was provided by Idaho State Univ. students Logan J. Tew, Dane Sterbentz, Bradley Heath, Izzi Silver, Bric Balmforth, Jari Safi, Jose Martinez, Randy Case and Ryan Loveland. DMM thanks Prof. Dr. C. J. Kähler and his colleagues at Uni. der Bundeswehr München for their gracious hospitality during multi-month technical visits in 2014 and 2018/2019 and Profs. T. A. Zaki of Johns Hopkins Univ. and K. P. Nolan of University College Dublin for making their tabulated temporal DNS results available. This study was partly supported by the Center for Advanced Energy Studies via U. S. Department of Energy Idaho Operations Office Contract DE-AC07-05ID14517 and by the U. S. DoE Office of Nuclear Energy's Nuclear Energy University Program (NEUP) via Contracts DE-AC07-05ID14517 (NEUP Project 10.876) and DE-NE0008965. Accordingly, the U.S. Government retains a nonexclusive, royalty-free license to publish or reproduce the published form of this contribution, or allow others to do so, for U.S. Government purposes.

References cited

Abraham, J. F., E. M. Sparrow, J. M. Gorman, Y. Zhao and W. J. Minkowycz, 2019. Application of an intermittency model for laminar, transitional and turbulent internal flows. *J. Fluids Engr.*, 141, pp. 071204-1 to -8.

Abraham, J. F., E. M. Sparrow and W. J. Minkowycz, 2011. Internal-flow Nusselt numbers for the low-Reynolds-number end of the laminar-to-turbulent transition regime. *Int. J. Heat Mass Transfer*, 54, pp. 584-588.

Abraham, J. F., E. M. Sparrow and J. C. K. Tong, 2009. Heat transfer in all pipe flow regimes: laminar, transitional/intermittent, and turbulent. *Int. J. Heat Mass Transfer*, 52, pp. 557-563.

Avila, M., D. Barkley and B. Hof, 2023. Transition to turbulence in pipe flow. *Annu. Rev. Fluid Mech.*, 55, pp. 575-602.

Bakewell, H. P., and J. L. Lumley, 1967. Viscous sublayer and adjacent wall region in turbulent pipe flow. *Phys. Fluids*, 10, pp. 1880-1889.

Bankston, C. A., 1970. The transition from turbulent to laminar gas flow in a heated pipe. *J. Heat Transfer,* 92, pp. 569-579.

Beavers, G. S., E. M. Sparrow and J. R. Lloyd, 1971. Low Reynolds number flow in large aspect ratio rectangular ducts. *J. Basic Engr*., 93, pp. 296-299.

Beavers, G. S., E. M. Sparrow and R. A. Magnuson, 1970a. Experiments on hydrodynamically developing flow in rectangular ducts of arbitrary aspect ratio. *Int. J. Heat Mass Transfer,* 13, pp. 689-701.

Beavers, G. S., E. M. Sparrow and R. A. Magnuson, 1970b. Experiments on the breakdown of laminar flow in a parallel-plate channel. *Int. J. Heat Mass Transfer,* 13, pp. 809-815.

Bejan, A., 1984. *Convection heat transfer*. New York: Wiley.

Birkhoff, G., and E. H. Zarantonello, 1957. *Jets, wakes and cavities*. New York: Academic Press.

Blackwelder, R. F., 1983. Analogies between transitional and turbulent boundary layers. *Phys. Fluids,* 28, pp. 2807-2815.

Blackwelder, R. F., and H. Eckelmann, 1979. Streamwise vortices associated with the bursting phenomenon. *J. Fluid Mech*., 94, pp. 577-594.

Blasius, H., 1913. Das Ähnlichkeitsgesetz bei Reibungsvorgängen in Flüssigkeiten. *Forsch. Arb. Ing.Wes*., No. 131, Berlin.

Boguslawski, L., and Cz. O. Popiel, 1979. Flow structure of the free round turbulent jet in the initial region. *J. Fluid Mech*., 90, pp. 531-539.

Bradshaw, P., R. B. Dean and D. M. McEligot, 1973. Calculations of interacting turbulent shear layers: Duct flow. *J. Fluids Eng*., 95, pp. 214-220.

Brandt, L., P. Schlatter and D. S. Henningson, 2004. Transition in boundary layers subject to free-stream turbulence. *J. Fluid Mech*., 517, pp. 167-198.

Carlson, D. R., S. E. Widnall and M. F. Peeters, 1982. A flow-visualization study of transition in plane Poiseuille flow. *J. Fluid Mech*., 121, pp. 487-505.

Choi, B.-H., N. K. Anand, Y. A. Hassan and P. Sabharwall, 2022. Large eddy simulation of flow through an axisymmetric sudden expansion. *Phys. Fluids*, 34, pp. 065117-1 to -13.

delPlace, F., 2018. Fluids flow stability in ducts of arbitrary cross-section. *J. Modern and Appl. Phys*., 2 (2), pp. 10-15.

Donaldson, C. duP., 1969. A computer study of an analytical model of boundary layer transition. *AIAA J.,* 7, pp. 271-278.

Durst, F., M. Fischer, J. Jovanovic and H. Kikura, 1998. Methods to set up and investigate low

Reynolds number, fully developed turbulent plane channel flows. *J. Fluids Engr.*, 120, pp. 496-503.

Durst, F., H. Kikura, I. Lekakis, J. Jovanovic and Q.Ye, 1996. Wall shear stress determination from near-wall mean velocity data in turbulent pipe and channel flows. *Exp. Fluids*, 20, pp. 417-428.

Eckelmann, H., 1974. The structure of the viscous sublayer and the adjacent wall region in a turbulent channel flow. *J. Fluid Mech.*, 65, pp. 439-459.

Eckhardt, B., T. M. Schneider, B. Hof and J. Westerweel, 2007. Turbulence transition in pipe flow. *Annu. Rev. Fluid Mech.*, 39, pp. 447-468.

Falkner, V. M., and S. W. Skan, 1931. Some approximate solutions of the boundary layer equations. *Philos. Mag.*, 12, pp. 865-896.

Finnis, M. V., and A. Brown, 1989. Stability of a laminar boundary layer flowing along a concave surface. *J. Turbo.*, 111, pp. 376-386.

Fischer, M., 1999. Turbulente wandgebundene Strömungen bei kleinen Reynoldzahlen. Ph.D. thesis, Uni. Erlangen, Deutschland.

Flügge-Lotz, I., and F. G. Blottner, 1962. Computation of the boundary-layer flow including displacement-thickness interaction using finite-difference methods. AFOSR 2206, Tech. Rpt. No. 131, Div. Engr. Mech., Stanford, January. Available from DTIC as AD No. 273 983.

Fukudome, K., and O. Iida, 2012. Turbulent-laminar patterns in Poiseuille and Couette flows. *Turbulence, Heat and Mass Transfer 7* (Ed.: K. Hanjalic, Y. Nagano, D. Borello and S. Jakirlic), New York: Begell House.

Gad-el-Hak, M., R. F. Blackwelder and J. J. Riley, 1981. On the growth of turbulent regions in laminar boundary layers. *J. Fluid Mech.,* 110, pp. 73-95.

Ghajar, A. J., and K. F. Madon, 1992. Pressure drop measurements in the transition region for a circular tube with three different inlet configurations. *Exp. Thermal Fluid Sci.*, 5, pp. 129-135.

Görtler, H., 1940. Über eine dreidimensionale instabilität laminarer grenzschichten an konckaven wänden. Ges. d. Wiss. Göttingen, Nachr. a.d. Math., Vol. 2(1). Also available as NACA-TM-1375.

Gottlieb, J. J., and D. V. Ritzel, 1979. A semi-empirical equation for the viscosity of air. DRES Suffield Tech. Note No. 454, July. Available from DTIC as AD No A-072053.

Hack, M. J. P., and T. A. Zaki, 2014. Streak instabilities in boundary layers beneath free-stream turbulence. *J. Fluid Mech.,* 741, pp. 280-315.

Hack, M. J. P., and T. A. Zaki, 2016. Data-enabled prediction of streak breakdown in pressure-gradient boundary layers. *J. Fluid Mech.,* 801, pp. 43-64.

Hashimoto, S., A. Hasobe, T. Tsukahara, Y. Kawaguchi and H. Kawamura, 2009. An experimental study on turbulent-stripe structure in transitional channel flows. *Turbulence, Heat and Mass Transfer 6* (Ed.: K. Hanjalic, Y. Nagano and S. Jakirlic) New York: Begell House, pp. 193-196.

He, S., and M. Seddighi, 2013. Turbulence in transient channel flow. *J. Fluid Mech.*, 715, pp. 60-102.

Herndon, D., E. J. Walsh and D. M. McEligot, 2007. Instantaneous fluctuation velocity and skewness distributions upstream of transition onset. *Int. J. Heat Fluid Flow,* 28, pp. 1272-1279.

Hershey, H. C., J. L. Zakin and R. Simha, 1967. Numerical differentiation of equally spaced and not equally spaced experimental data. *I&EC Fundamentals*, 6, No. 3, pp. 413-421. See H. C. Hershey letter dated 22 Feb. 1968 for corrections to Table III.

Hilsenrath, J., C. W. Beckett, W. S. Benedict, L. Fano, H. J. Hoge, J. F. Masi, R. L. Nuttall, S. Touloukian and H. W. Woolley, 1955. *Tables of thermal properties of gases*. N.B.S. Circular 564, Washington: U.S. Government Printing Office.

Holman, S. W., 1886. On the effect of temperature on the viscosity of air and carbon dioxide. *London, Edinburgh and Dublin Philosoph. Mag. and J. Science*, 21 (130) Article no. XXIX, pp. 199-222.

Idelchik, I.E., 1994. *Handbook of hydraulic resistance, 3rd ed*. Boca Raton, Florida: CRC Press, Inc.

Jackson, D., and B. Launder, 2007. Osborne Reynolds and the publication of his papers on turbulent flow. *Annu. Rev. Fluid Mech.*, 39, pp. 19-35.

Jeong, J., F. Hussain, W. Shoppa and J. Kim, 1997. Coherent structures near the wall in a turbulent channel flow. *J. Fluid Mech.*, 332, pp. 185-214.

Jiang, N., and T. W. Simon, 2005. Transition in low-pressure turbines: Effects of unsteady acceleration and turbulence intensity. *J. Thermophys. and Heat Transfer*, 19. pp. 148-155.

Johnson, R. W., 1998. *The handbook of fluid dynamics*. Berlin: Springer.

Johnson, R. W., 2011. Pre-test CFD calculations for a bypass flow standard problem. ASME paper IMECE2011-65831. Also available as INL/CON-11-20931 from inldigitallibrary.inl.gov/STI/5223012.pdf.

Johnson, R. W., and H. Sato, 2010. Bypass flow computations using a one-twelfth symmetric sector for normal operation in a 350 MWth prismatic VHTR. Paper 152, HTR2010, Prague, October.

Kähler, C. J., 2014. Personal communication. Seminar, Institut für Strömungsmechanik und Aerodynamik, Uni. der Bundeswehr München, December.

Kakac, S., R. K. Shah and W. Aung, 1987. *Handbook of single-phase convective heat transfer*. New York: John Wiley and Sons.

Kasagi, N., M. Hirata and K. Nishino, 1986. Streamwise pseudo-vortical structures and associated vorticity in the near-wall region of a wall-bounded turbulent shear flow. *Exp. Fluids*, 4, pp. 309-318.

Kays, W. M., 1966. *Convective heat and mass transfer*. New York: McGraw-Hill.

. Klebanoff, P. S., 1971. Effect of freestream turbulence on the laminar boundary layer. *Bull., Amer. Phys. Soc.,* 10(11), p. 1323.

Klebanoff, P. S., K. D. Tidstrom and L. M. Sargent, 1962. The three-dimensional nature of boundary-layer instability. *J. Fluid Mech.*, 12, pp. 1-34.

Kleiser, L., and T. A. Zang, 1991. Numerical simulation of transition in wall-bounded shear flows. *Annu. Rev. Fluid Mech.*, 23, pp. 495-537.

Kline, S. J., W. C. Reynolds, F. A. Schraub and P. W. Rundstadler, 1967. The structure of turbulent boundary layers. *J. Fluid Mech.*, 30, pp. 741-773.

Kohyama, K., M. Sano and T. Tsukahara, 2022. Sidewall effect on turbulent band in subcritical transition of high-aspect ratio duct flow. *Phys. Fluids*, 34, pp. 084112-1 to -24.

Lagha, M., 2007. Turbulent spots and waves in a model for plane Poiseuille flow. *Phys. Fluids*, 19, pp. 124103-1 to -10.

Lardeau, S., N. Li and M. A. Leschziner, 2007. Large eddy simulation of transitional boundary layers at high free-stream turbulence intensity and implications for RANS modeling. *J. Turbomachinery*, 129, pp. 311-317.

Launder, B. E., 1963. The turbulent boundary layer in a strongly negative pressure gradient. Master's thesis, MIT. Also MIT Gas Turbine Lab. Rpt. 71. Condensed version available as: Laminarization of the turbulent boundary layer in a severe acceleration. *J. Appl. Mech.*, 31, No. 4, pp. 707-708, December 1964.

Launder, B. E., 1964. Laminarization of the turbulent boundary layer by acceleration. MIT Gas Turbine Lab. Rpt. 77. Also NASA N66-16042.

Launder, B. E., and N. D. Sandham (eds.), 2002. *Closure strategies for turbulent and transitional flows*. Cambridge: Univ. Press.

Lee, C., and X. Jiang, 2019. Flow structures in transitional and turbulent boundary layers. *Phys. Fluids,* 31, pp. 111301-1 to -40.

Marxen, O., and T. A. Zaki, 2019. Turbulence in intermittent transitional boundary layers and in turbulent spots. *J. Fluid Mech.,* 860, pp. 350-383.

Matsubara, M., S. Horii, Y. Sagawa, Y. Takahashi and D. Saito, 2016. Very-large-scale fluctuations in turbulent channel flow at low Reynolds numbers. *Int. J. Heat Fluid Flow*, 62, pp. 593-597.

Mayle, R. E., 1991. The role of laminar-turbulent transition in gas turbine engines. *J. Turbomachinery*, 113, pp. 509-537.

McCreery, G. E., 2012. Personal electronic communication. Mech. Engr. Dept., Idaho State Univ., 16 January.

McCreery, G. E., 2023. Personal electronic communication. Idaho Falls, Ida., 19 April.

McCreery, G. E., 2023. Personal electronic communication. Idaho Falls, Ida., 11 May.

McCreery, G. E., , L. J. Tew, B. G. Williams, R. R. Schultz and D. M. McEligot, 2013. MHTGR core bypass flow patterns and pressure losses. NuReTH-15-146, Pisa, 12-15 May. Also available as INL/CON-12-278335 from inldigitallibrary.inl.gov/sti/5737953.pdf

McEligot, D. M., R. S. Brodkey and H. Eckelmann, 2009. Laterally converging duct flows: Part 4. Temporal behavior in the viscous layer. *J. Fluid Mech.,* 634, pp. 433-461.

McEligot, D. M., X. Chu, J. H. Bae, E. Laurien and J. Y. Yoo, 2020. Some observations concerning "laminarization" in heated vertical tubes. *Int. J. Heat Mass Transfer,* 163, pp. 120101-1 to -16. Available via doi.org/10.1016/j.ijheatmasstransfer.2020.120101

McEligot, D. M., C. W. Coon and H. C. Perkins, 1970. Relaminarization in tubes. *Int. J. Heat Mass Transfer*, 13, pp. 431-433.

McEligot, D. M., and H. Eckelmann, 2006. Laterally converging duct flows: Part 3. Mean turbulence structure in the viscous layer. *J. Fluid Mech.*, 549, pp. 25-59.

McEligot, D. M., and R. W. Johnson, 2017. Bypass flow resistance in prismatic gas-cooled nuclear reactors. *J. Nuc. Eng. and Radiation Sci.,* 3, No. 1, pp. 011003-1 to-9. Available via nuclearengineering.asmedigitalcollection.asme.org/.

McEligot, D. M., K. P. Nolan, E. J. Walsh and T. A. Zaki, 2024. Entropy generation in bypass transition with streamwise pressure gradients. Manuscript in preparation.

Melese, G., and R. Katz, 1984. *Thermal and flow design of helium-cooled reactors*. la Grange Park, Ill.: American Nuclear Society.

Menter, F. R., R. B. Langtry, S. R. Likki, Y. B. Suzen, P. G. Huang and S. Folker, 2004. A correlation-based transition model using local variables. Part I – Model formulation. Proc., Int. Gas Turbine Conf., Wien, 14-17 June.

Minkowycz, W. J., J. P. Abraham and E. M. Sparrow, 2009. Numerical simulation of laminar breakdown and subsequent intermittent and turbulent flow in parallel-plate channels: Effects of inlet velocity profile and turbulence intensity. *Int. J. Heat Mass Transfer*, 52, pp. 4040-4046.

Miyazaki, M., 2014. Effect of nano-fibrillated cellulose suspension on transitional two-dimensional channel flow. M.Sc. thesis, Shinshu U., Japan.

. Morkovin, M. V., 1969. On the many faces of transition. *Viscous Drag Reduction* (Ed.: C. S. Wells), New York: Plenum, pp. 1–31.

Mullin, T., 2011. Experimental studies of transition to turbulence in a pipe. *Annu. Rev. Fluid Mech.*, 39, pp. 1-24.

Murphy, H. D., F. W. Chambers and D. M. McEligot, 1983. Laterally converging flow. I: Mean flow. *J. Fluid Mech.*, 127, pp. 379-401.

Muzychka, Y. S., and M. M. Yovanovich, 2009. Pressure drop in laminar developing flow in noncircular ducts: A scaling and modeling approach. *J. Fluids Engr.*, 131, pp. 111105-1 to -11.

Narasimha, R., and K. R. Sreenivasan, 1979. Relaminarization of fluid flows. *Adv. Appl. Mech.*, 19, pp. 221-309.

Nolan, K. P., and T. A. Zaki, 2013. Conditional sampling of transitional boundary layers in pressure gradients. *J. Fluid Mech.* , 728, pp. 306-339.

Orlandi, P., and S. Pirozzoli, 2020. DNS of transitional and turbulent flows in rectangular ducts: budgets and projection in principal mean strain rates. *J. Turbulence*, 21 (5-6), pp. 286-310.

Owolabi, B. E., 2018. Characterisation of turbulent duct flows: experiments and direct numerical simulations. Ph.D. thesis, U. Liverpool, October.

Pacciani, R., M. Marconcini, A. Fadi-Ghotbi, S. Lardeau and M. A. Leschziner, 2009. Calculations of high-lift cascades in low-pressure turbine conditions using a three-equation model. Paper GT2009-59557, ASME Turbo Expo, Orlando, 8-12 June.

Patel, V. C., and M. R. Head, 1969. Some observations on skin friction and velocity profiles in fully developed pipe and channel flows. *J. Fluid Mech.*, 38, pp. 181-201.

Qui, S., and T. W. Simon, 1997. An experimental investigation of transition as applied to low pressure turbine suction surface flows. ASME paper 97-GT-455.

Rehman, D., G. L. Morini and C. Hong, 2019. A comparison of data reduction methods for average friction factor calculation of adiabatic gas flows in microchannels. *Micromachines*, 10, No. 3, pp. 171-1 to -18.

Rehman, D., F. Vignati, C. Hong and G. Morini, 2019. Laminar to turbulent flow transition in a rectangular duct with 1:10 aspect ratio using DNS and RANS transitional turbulence model. Proc., Int. Symp. Thermal Effects on Gas flows In Microscale (ISTEGIM), Erlangen, 24-25 October.

Rehill, B., E. J. Walsh, P. Schlatter, L. Brandt, T. Zaki and D. M. McEligot, 2013. Identifying turbulent spots in transitional boundary layers. *J. Turbomachinery*, 146, pp. 011019-1 to -8.

Reynolds, O., 1883. An experimental investigation of the circumstances which determine whether the motion of water shall be direct or sinuous and of the law of resistance in parallel channels. *Philos. Trans., Royal Soc. London Ser. A,* 174, pp. 935-982.

Rohsenow, W. M., and J. P. Hartnett, 1973. *Handbook of heat transfer*. New York: McGraw-Hill.

Rotta, J. C., 1956. Experimenteller Beitrag zur Entstehung turbulenter Strömung im Rohr. *Ing. Arch.*. Bd. 24, pp. 258-281.

Sankaran, R., M. Sokolov and R. A. Antonia, 1988. Substructures in a turbulent spot. *J. Fluid Mech.*, 197, pp. 389-414.

Sankaran, R., R. A. Antonia, D. K. Bisset and M. Sokolov, 1991. Flow patterns and organization within a turbulent spot. *Phys. Fluids A*, 3 (6), pp. 1560-1571.

Savill, A. M., 1993. Some recent progress in the turbulence modeling of by-pass transition. *Near-Wall Turbulent Flows* (Eds.: R. M. C. So and B. E. Launder), New York: Elsevier, pp. 829-848.

Savill, A. M., 2002a. By-pass transition using conventional closures. *Closure strategies for turbulent and transitional flows*. (Eds.: B. E. Launder and N. D. Sandham), Ch. 17, Cambridge: Univ. Press, pp. 464-492.

Savill, A. M., 2002b. New strategies in modeling by-pass transition. *Closure strategies for turbulent and transitional flows*. (Eds.: B. E. Launder and N. D. Sandham), Ch. 18, Cambridge: Univ. Press, pp. 493-521.

Sano, M., and K. Tamai, 2016. A universal transition to turbulence in channel flow. *Nat. Phys.*, 12, pp. 249-253.

Schade, K. W., and D. M. McEligot, 1971. Cartesian Graetz problems with air property variation. *Int. J. Heat Mass Transfer*, 14, pp. 653-666.

Schlichting, H., 1968. *Boundary layer theory, 6th ed*. New York: McGraw-Hill.

Schlichting, H., and K. Gersten, 2000. *Boundary layer theory, 8th revised and enlarged ed*. Berlin: Springer.

Schumacher, J., and B. Eckhardt, 2001. Evolution of turbulent spots in a parallel shear flow. *Phys. Rev. E*, 63 (4 II), pp. 463071-463079.

Scorer, R. S., 1967. Local instability in curved flow. *IMA J. Appl. Math.*, 3 (3), pp. 250-265.

Seki, D., and M. Matsubara, 2012. Experimental investigation of relaminarizing and transitional channel flows. *Phys. Fluids*, 24, pp. 124102-1 to -23.

Shah, R. K., and A. L. London, 1978. *Laminar flow forced convection in ducts*. New York: Academic Press.

Smits, A. J., N. Matheson and P. N. Joubert, 1983. Low-Reynolds-number turbulent boundary layers in zero and favorable pressure gradients. *J. Ship Research*, 27, pp. 147-157.

Spalart. P. R., 1986. Numerical study of sink-flow boundary layers. *J. Fluid Mech.*, 172, pp. 307-328.

Sutherland, W., 1893. The viscosity of gases and molecular force. *Philosophical Mag. Series 5*, 36 (223), Article no. LII, pp. 507-531.

Takeishi, K., G. Kawahara, H. Wakabayashi, M. Uhlmann and A. Pinelli, 2015. Localized turbulence structures in transitional rectangular-duct flow. *J. Fluid Mech.*, 782, pp. 368-379.

Tew, L. J., 2013. Investigation of plenum flow behavior with different entrance and exit geometries. M.S. thesis, Mech. Engr., Idaho State Univ., 15 July.

Tew, L. J., 2023. Personal electronic communication. Idaho Falls, Ida., 4 May.

Tew, L. J., 2023. Personal electronic communication. Idaho Falls, Ida., 27 May.

Thwaites, B., 1949. Approximate calculation of the laminar boundary layer. *Aero. Quarterly*, 1, pp. 245-280.

Tosun, I., D. Uner and C. Ozgen, 1988. Critical Reynolds number for Newtonian flow in rectangular ducts. *Ind. Eng. Chem. Res.*, 27, pp. 1955-1957.

Tsukahara, T., Y. Seki, H. Kawamura and D. Tochio, 2004. DNS of turbulent channel flow with very low Reynolds numbers. *Computational Mechanics*, WCCM VI, Beijing, China.

Tsukahara, T., Y. Seki, H. Kawamura and D. Tochio, 2004. DNS of turbulent heat transfer at very low Reynolds numbers. Proc., 1st Int. Forum Heat Transfer, Kyoto, November.

Tsukahara, T., Y. Seki, H. Kawamura and D. Tochio, 2005. DNS of turbulent channel flow at very low Reynolds numbers. *Proc., 4th Int. Symp. Turb. Shear Flow Phen.*, pp. 935-940.

Tuckerman, L. S., M. Chantry and D. Barkley, 2020. Patterns in wall-bounded shear flows. *Annu. Rev. Fluid Mech.*, 52, pp. 341-367.

Turner, C., and R. Prosser, 2009. The application of laminar kinetic energy to laminar-turbulent transition prediction. *Turb. Heat Mass Transfer*, 6, pp. 209-212.

Uhlmann, M., A. Pinelli, G. Kawahara and A. Sekimoto, 2007. Marginally turbulent flow in a square duct. *J. Fluid Mech.*, 588, pp. 153-162.

van Driest, E. R., 1952. Investigation of laminar boundary layer in compressible fluids using the Crocco method. NACA TN 2597, January.

Vinuesa, R., A. Noorani, A. Lozano-Duran, G. K. el Khoury, P. Schlatter, P. F. Fischer and H. M. Nagib, 2014. Aspect ratio effects in turbulent duct flows studied through direct numerical simulations. *J. Turbulence*, 15 (10), pp. 677-706.

Walsh, E. J., D. M. McEligot, L. Brandt and P. Schlatter, 2011. Entropy generation in boundary layers transitioning under the influence of freestream turbulence. *J. Fluids Engr.*, 133, pp. 061203-1 to -10.

Walters, D. K., and D. Cokljat, 2008. A three-equation eddy-viscosity model for Reynolds-averaged Navier-Stokes simulations of transitional flow. *J. Fluids Engr.,* 130, pp. 121401-1 to -14.

Watanabe, K., S. Akaoka, M. Matsubara and M. Kvick, 2012. Statistical properties of disturbances in transitional channel flow. Proc., 9th Int. Conf. Fluid Dyn, Sendai, 19-21 September.

White, F. M., 1991. *Viscous fluid flow, 2nd edition*. Boston: McGraw-Hill.

Williams, B. G., 2014. Personal electronic communication. Mech. Engr. Dept., Idaho State Univ., 25 February.

Williams, B. G., 2015. Studies of deteriorated heat transfer in prismatic cores stemming from irradiation-induced geometry distortion. Final technical report, Project 10.876, U.S. DoE Nuclear Energy University Program, Mech. Engr. Dept., Idaho State Univ., August. Available as www.osti.gov/biblio/1214656.

Wu, X., 2023. New insights into turbulent spots. *Annu. Rev. Fluid Mech.*, 55, pp. 45-75.

Wu, X., P. Moin, J. M. Wallace, J. Skarda, A. Lozano-Duran and J.-P. Hickey, 2017. Transitional-turbulent spots and turbulent-turbulent spots in boundary layers. *Proc., Nat. Acad. Sci.*, 114 (27), pp. E5292-E5299.

Wygnanski, I. J., and F. H. Champagne, 1973. On transition in a pipe. Part 1. The origin of puffs and slugs and the flow in a turbulent slug. *J. Fluid Mech.*, 59, pp. 281-335

Yimprasert, S., M. Kvick, P. H. Alfredsson and M. Matsubara, 2021. Flow visualization and skin friction determined in transitional channel flow. *Exp. Fluids*, 62, pp. 31-1 to -16.

Zaki, T. A., 2010. Bypass transition to turbulence and the anatomy of turbulent spots. Final report, Mech. Engr., Imperial College, London, July. Available from DTIC as ADA531085.

Zaki, T. A., 2013. From streaks to spots and on to turbulence: exploring the dynamics of boundary layer transition. *Flow, turbulence and combustion*, 91, pp. 451-473.

Zanoun, E.-S., M. Kito and C. Egbers, 2009. A study of flow transition and development in circular and rectangular ducts. *J. Fluids Engr.*, 131(6) pp. 061204-1 to -10.

Zanoun, E.-S., H. Nagib and F. Durst, 2009. Refined c_f relation for turbulent channels and consequences for high-Re experiments. *Fluid Dyn. Res.*, 41, pp. 021405-1 to -12.